Integration and optimization of methanol-reforming proton exchange membrane fuel cell system for distributed generation with combined cooling, heating and power

Zheng Liang[1], Yingzong Liang[1, 2, *], Xianglong Luo[1, 2, **], Huasheng Wang[3], Wei Wu[4], Jianyong Chen[1, 2], Ying Chen[1, 2]

[1] School of Materials and Energy, Guangdong University of Technology, Guangzhou, China

[2] Guangdong Province Key Laboratory on Functional Soft Matter, Guangdong University of Technology, Guangzhou, China

[3] School of Engineering and Materials Science, Queen Mary University of London, London E1 4NS, UK

[4] School of Energy and Environment, City University of Hong Kong, Hong Kong, China

May 1, 2024

Submitted to *Journal of Cleaner Production*

Abstract

The methanol-steam-reforming proton exchange membrane fuel cell system is an attractive option for distributed cogeneration due to its low emissions, quiet operation, and low-cost fuel storage. To further increase its energy efficiency, waste heat can be utilized for combined cooling, heating, and power generation. However, the additional equipment, processes, and streams required for cogeneration make the system design complex, with a large number of degrees of freedom. To address this challenge, we propose an equation-based optimization framework for the simultaneous heat integration and flowsheet optimization of the combined cooling, heating, and power system based on the methanol-steam-reforming proton exchange membrane fuel cell. The framework comprises a detailed modelling of methanol steam reforming reaction, fuel cell performance, cooling/heating cogeneration systems, heat integration, heat exchanger network synthesis and energetic-economic performance evaluation. Additionally, the framework incorporates the sizing of the corresponding equipment, including the total length of the reformer, scale of proton exchange membrane fuel cell stack, and absorption cooling apparatus. Furthermore, it takes into account the operating conditions, such as the temperature and pressure of methanol steam reforming reaction, the operating temperatures and pressures of

[*,**]Corresponding authors. Email: yliang@gdut.edu.cn (Y. Liang), lxl-dte@gdut.edu.cn (X. Luo).

the fuel cell stack and absorption cooling system. We apply the framework to a 1,000 kWe combined cooling, heating, and power generation system, and the integrated design achieved an energy efficiency of 88.50% and a levelized cost of electricity of 0.2374 $/kWh. The results show that the simultaneous heat integration and flowsheet optimization can increase the system's energy efficiency by 5.45 percentage points, exergy efficiency by 2.22 percentage points, and decrease the levelized cost of electricity by 4.50% compared to a conventional design.

Keywords: Distributed generation, methanol-steam-reforming, proton exchange membrane fuel cell, combined cooling-heating-power generation, simultaneous heat integration and flowsheet optimization.

1. Introduction

Energy reform is usually at the top of the agenda for fending off the worsening effect of rising temperature when discussing climate change (BP, 2022). Recent geopolitical conflict not only triggered a short-term spike in energy prices, but also could prompt a long-term shift towards more sustainable sources and higher efficient systems (Wang et al., 2020; Liang et al., 2021a). Distributed generation becomes increasingly prominent in power generation for its compatibility with advanced generation techniques (e.g. fuel cell) utilizing renewable fuels (e.g. hydrogen and methanol) (Xu et al., 2015; Jin et al., 2019). Though the efficiency of such system for sole power is generally lower than that of the centralized generation system, the distributed generation often achieves higher cogeneration efficiency by combined heating and power (CHP) or combined heating, cooling and power (CCHP) generation due to its proximity to end users (Gao et al., 2014; Sun et al., 2019). As more and more distributed generation plants will be built in the foreseeable future, it would be an achievement if effective tools for system design and optimization can be developed to improve the economic and energy performances of distributed systems.

CHP/CCHP systems can be categorized based on their prime movers (e.g. fuel cells (Sun et al., 2021), solar collectors (Liu et al., 2018), biomass boilers (Su et al., 2020), turbines (Zhao et al., 2019)). Particularly, fuel cell is one of the most promising prime movers applied in the CHP/CCHP system on account of its high energy density, superior conversion efficiency, and low emission (Wu et al., 2020). Solid oxide fuel cell (SOFC) and proton exchange membrane fuel cell (PEMFC) dominate in fuel cell-based trigeneration systems (Ellamla et al., 2015). Recently, there are some published reviews on the application of SOFC-based trigeneration

system (Buonomano et al., 2015; Radenahmad et al., 2020). However, SOFC usually operates at a high temperature (400-700℃) and emits carbon dioxide. By contrast, with an operating temperature lower than 250℃, zero greenhouse gas emission and a shorter start-up time, PEMFC is more desirable for a manageable, environmentally-friendly and flexible CCHP system. Chen et al. (2015) proposed a 5 kW PEMFC-based residential micro-CCHP system and conducted an analysis of its operating performance in summer and winter. Their results showed that the system could achieve 70.1% efficiency at maximum in summer and 82% at maximum in winter. Chang et al. (2017a) investigated a high-temperature PEMFC-based micro CCHP system, which performed an average coefficient of performance (COP) of 1.19 in summer and 1.42 in winter. They suggested that the system had a good prospect for residential application. Fan et al. (2022) applied a PEMFC-based CHP system to produce electricity and heat for an eco-neighborhood in North China with low greenhouse gas emissions, and its performance in eco-neighborhood scenario under the electricity-led and thermal-led strategies was investigated. Zhao et al. (2022a) adopted a novel PEMFC-based CCHP system for data center with high humidity requirements and analyzed the dynamic characteristics and economic performance. They pointed out that the scheme with parabolic trough solar collector as an auxiliary heat source could save about 62 kg of hydrogen per day. Then, they proposed a multi-stack coupled power supply strategy to relieve the power fluctuation of CCHP system (Zhao et al., 2022b). More research progress on PEMFC-based multigeneration systems can be found in (Arsalis, 2019; Baroutaji et al., 2021).

Hydrogen has been widely accepted as a premium energy source for fuel cell-based CHP/CCHP system. However, it is a challenging task to transport and store hydrogen due to its inflammability and explosiveness (Safari et al., 2020). Thus, manageable hydrogen source is acknowledged as a bottleneck in the development of fuel cell-based CHP/CCHP system. In recent years, studies on CHP/CCHP systems integrated with hydrogen production and utilization have gained traction (Zhao et al., 2022c). As reported by Clarivate, there are currently over 100 publications specifically focused on fuel cell-based CHP/CCHP systems integrated with hydrogen production. Such hydrogen production facility can be in the form of a fuel processing system, generating hydrogen from fuels, such as natural gas and methanol, or in the form of an electrolyzer for on-site generation of hydrogen from water (Baroutaji et al., 2021). Xie et al. (2012) proposed a PEMFC-based CCHP system integrated with a natural gas processing unit, in which hydrogen-rich syngas was generated through autothermal reforming reaction. Jannelli et al.

(2013) focused on a micro-cogeneration system, which consisted mainly of a natural gas steam reforming, a power unit, and a PEMFC. A maximum energy efficiency of 80% was obtained by the system based on low-temperature PEMFC. Loreti et al. (2021) investigated a hybrid gas turbine and PEMFC-based CHP system, in which the fuel processor relied on partial oxidation. They stated that the system achieved an overall efficiency higher than 85%. Al-Nimr et al. (2017) proposed a CCHP system integrated with geothermal cooling and an electrolyzer/fuel cell storage unit, in which electricity was generated by the organic Rankine cycle and fuel cell, and the electrolyzer took charge of the hydrogen production. They found that the system was improved in its overall power generation efficiency by 15.72%-17.78%. Taking into account the differences among various hydrogen production methods, Ercolino et al. (2015) conducted the performance evaluation and comparison of fuel processors integrated with PEMFC. They concluded steam reforming-based methods achieved higher efficiency than autothermal reforming-based methods. In fact, methanol steam reforming (MSR) is often considered a better choice because of its lower cost and higher efficiency (Authayanun et al., 2014; Chen et al., 2018a). In addition, methanol, which is a liquid at atmospheric temperature, requires less storage space and is more suitable for the distributed energy system, compared with natural gas. Wang et al. (2017) proposed a fuel cell-based trigeneration system integrated with MSR powered by solar thermal energy, whose energy and exergy efficiencies in summer could be up to 73.7% and 51.7%, respectively. Sarabchi et al. (2019) examined a PEMFC stack-based cogeneration system integrated with a solar methanol steam reformer and a Kalina cycle. They found that the average daily exergy efficiency was increased by 29.3%, while the total product unit cost and specific carbon dioxide emission were cut down by 17.72% and 16.3%, respectively. Chen et al. (2020) presented a micro-CCHP system integrated with geothermal-driven methanol reforming PEMFC stack. Their research results showed that the novel system achieved an energy efficiency of 66.3% and a levelized cost of energy at 0.0422 $/kWh.

While integrating hydrogen production process with CCHP systems is energetically advantageous, the designs are complicated due to the complex tradeoffs among large numbers of design variables. As such, much effort has been dedicated to the modeling and optimization to maximize performance of the systems. Asensio et al. (2017) applied artificial neural network to conduct the performance evaluation of a PEMFC-based CHP system, and trained an artificial neural network on a PEMFC-based cogeneration system through numerical tests. The results

showed the model achieved high accuracy in predicting performance of the real-world system, and they concluded that the model was suitable for techno-economic efficiency optimization. Mamaghani et al. (2016) utilized genetic algorithm to perform a multi-objective optimization of a PEMFC-based CHP system with the objectives of the net electrical efficiency and total capital cost. They obtained an efficiency-economics balanced design with a cumulative net electrical efficiency of 27.07% and a capital cost of 68,398 €. Subsequently, they adopted primary energy saving index to search for the best operating point in terms of electrical and thermal efficiencies. It was found that the system could operate with a net electrical efficiency up to 32.3% and a thermal efficiency of 61.1% through the optimization (Mamaghani et al., 2018). Chen et al. (2018b) performed a comprehensive multi-criteria analysis on a 5 kW PEMFC-based CCHP system, which encompassed aspects related to thermodynamics, economics, and environmental impact. This assessment was conducted through the utilization of a multi-objective non-dominated sorting genetic algorithm-II (NSGA-II). Results showed that the system achieved an exergy efficiency of 39.9%, an annual cost of $29,337.3, and a greenhouse gas emission reduction of 18,200 kg at the final optimal design. Zhao et al. (2021) developed a multi-objective optimization algorithm incorporated with the NSGA-II and ideal solution (TOPSIS) method to evaluate performances of a novel PEMFC-based CCHP system applied to data centers. Results indicated that the optimization led to significant improvement in energetic, exergetic, economic and environmental performances, compared with the non-optimized system.

Although much has been done to optimize the design and operating variables (e.g. reaction temperature) of distributed generation systems with fixed layouts, few studies have been dedicated to simultaneous heat integration and process optimization in the field of PEMFC-based CCHP. In general, a predetermined structure may restrict potential heat integration within the system, leading to suboptimal design with higher energy cost and lower efficiency (Liang et al., 2021b; Liang et al., 2022a). Thus, there is a strong incentive to optimize both the operating conditions and heat integration/heat exchange networks (HENs) of distributed generation systems. To the best of our knowledge, no published literature by far has been found that investigates simultaneous heat integration and process optimization of the CCHP system with methanol steam reforming and PEMFC.

Major contributions of this study are summarized as follows.

- A mixed-integer nonlinear programming (MINLP) framework for methanol steam reforming PEMFC-based CCHP system design is presented. The framework enables multi-variate optimization ranging from equipment sizing and investment costs on reformer, fuel cell stack and heat exchanger and so on, to operating conditions and costs, such as reaction temperature and pressure, and raw material consumption.
- Heat integration model is embedded into the framework, along with equation of state for thermodynamic properties estimation (e.g. enthalpy and entropy) and unit operation models for physical/chemical process calculation (e.g. vapor-liquid separation and chemical reaction kinetics), to realize simultaneous heat integration and flowsheet optimization for the purpose of increasing energy conversion efficiency and reducing investment and operating cost.
- As for the MINLP model, a tailored multi-step initialization procedure is designed for boosting its solution efficiency, and a multi-start algorithm is developed to improve its solution quality.
- A case study on distributed generation system design is presented to demonstrate the energy efficiency of the proposed CCHP system with process integration and to illustrate the effectiveness of the proposed optimization approach for complex system design.

The paper starts with a formal problem statement (Section 2), in which the description of methanol-steam-reforming PEMFC-based CCHP system is given and the difficulties in realizing simultaneous heat integration and flowsheet optimization are discussed. The optimization framework with detailed models of the MSR process, PEMFC, and absorption cooling will be presented in Section 3, along with the superstructure model for the HEN synthesis that realizes the energy target. The initialization procedure and multi-start optimization algorithms that resolve the computational difficulties in solving the proposed framework will be discussed in Section 4. A case study on a 1,000-kWe distributed generation system design will be presented in Section 5 to demonstrate the cost-effectiveness of the proposed integrated design in comparison with a conventional design. Comprehensive analysis of the integrated system will also be included. Finally, conclusions will be drawn in Section 6.

2. Problem statement

In this section, we present a formal statement of the flowsheet design and heat integration problem for CCHP systems based on methanol-reforming PEMFC addressed in this study.

Fig. 1 shows the schematic of a conventional CCHP system with methanol-reforming PEMFC (C-CCHP (Chen et al., 2015)). This system will serve as a baseline case for comparison with the proposed integrated design. It mainly comprises an MSR subsystem, a PEMFC stack, a pressure swing adsorption (PSA) subsystem, and a lithium bromide absorption cooling subsystem. Methanol/water mixture from the fuel tank is sent to the pump and pressurized, preheated in the heat exchanger, and subsequently superheated at the superheater. The high-temperature reactants are transformed into a hydrogen-rich mixture with unreacted methanol, water vapor, carbon monoxide, and carbon dioxide in the MSR subsystem. Thermal energy of the MSR subsystem effluent is recovered by the reactant feed of MSR subsystem, and the effluent further cools down in the condenser. The cooled products are sent to the separator, where the unreacted methanol and water are recycled and mixed with the fresh methanol/water. On the other hand, the syngas flows into the PSA system and is refined to make pure hydrogen. The pure hydrogen product is sent to the preheater and then to PEMFC stack to generate electricity. Finally, the reaction heat produced from the PEMFC is recuperated by the single effect absorption cooling (AC) system to produce hot water and cold water.

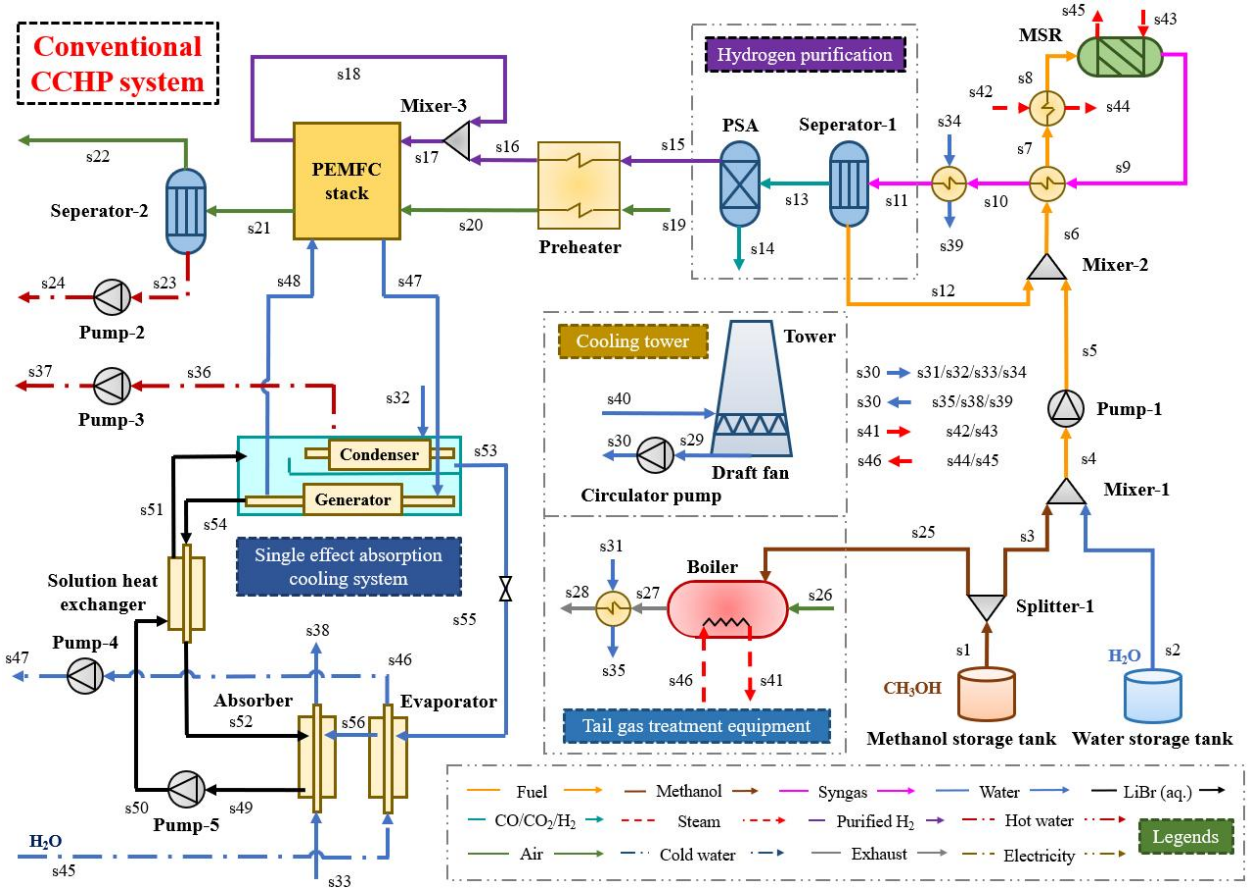

Fig. 1 Schematic flowsheet of conventional methanol-reforming PEMFC-based CCHP system.

Fig. 2 displays the proposed CCHP system with process integration (PI-CCHP). Here, the system can be categorized into six modules, namely a raw material supply and hydrogen purification subsystem, a methanol-steam-reforming PEMFC, a single effect absorption cooling subsystem, tail gas treatment equipment, process streams integration and a cooling tower. The PI-CCHP system differs from the C-CCHP system in terms of its integration strategy. Here, the process streams integration module acts as a "bridge" that connects each subsystem. Specifically, the PI-CCHP system allows match of all potential heat exchange streams, unlike the traditional C-CCHP system that only performs heat recovery between reactants and products of the MSR system. For example, the unreacted hydrogen as purge gas, products of the MSR system and combustion products from the boiler in PI-CCHP system are considered as hot streams of which thermal energy can be recovered. The cold streams include air, reactants of the MSR subsystem and purified hydrogen from the PSA subsystem. Furthermore, the tail gas treatment equipment is a boiler in either the C-CCHP system or the PI-CCHP system that generates steam as hot utility

by burning tail gas consisting of carbon monoxide, carbon dioxide, and hydrogen. Insufficient heat will be supplemented by methanol combustion.

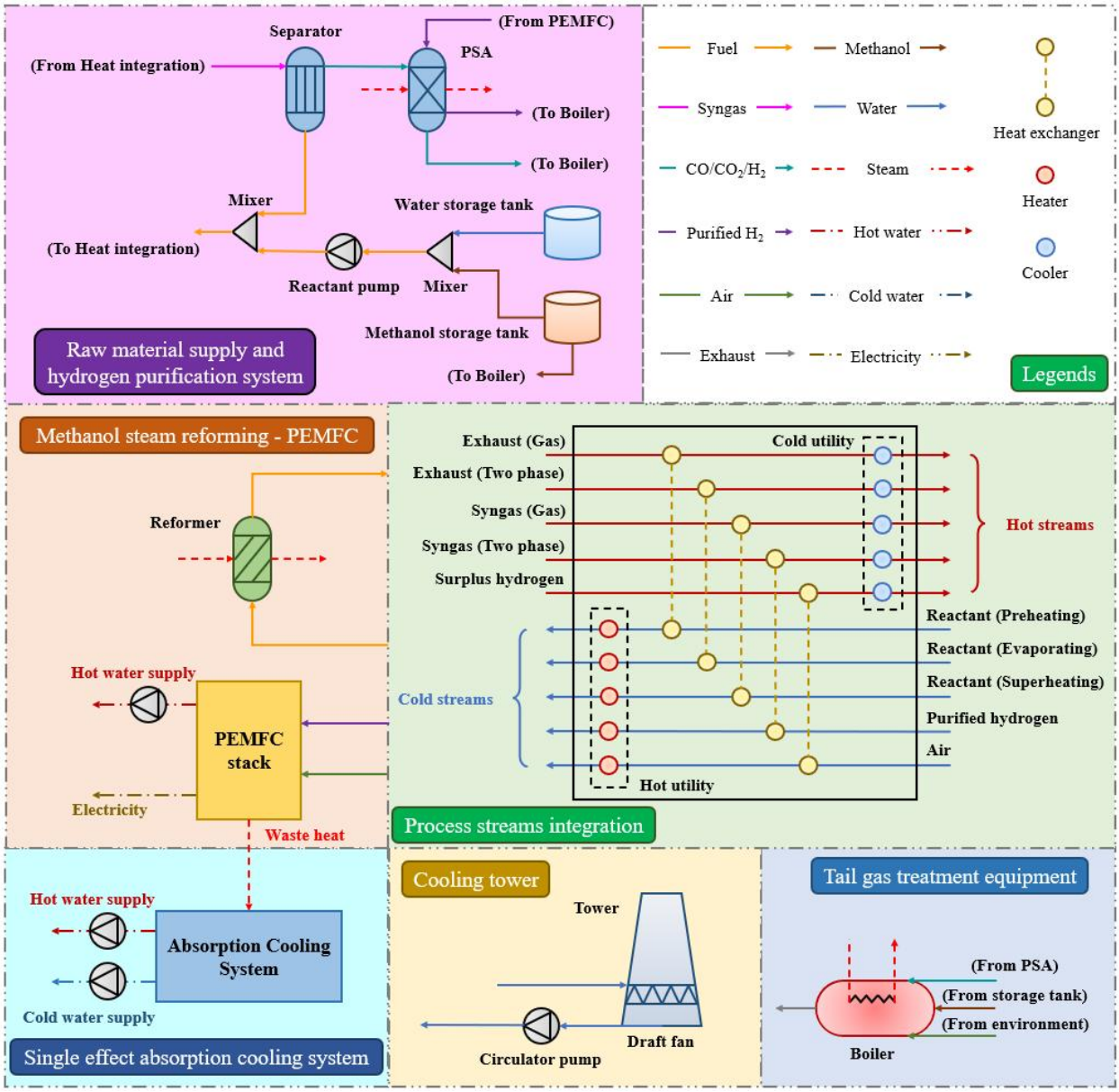

Fig. 2 Schematic of the proposed CCHP system with process streams integration (PI-CCHP).

This study optimized a 1,000-kWe scale CCHP system for efficient energy operation, and evaluated its ability to provide electricity, heating, and cooling to over 300 households. The study also conducted a comparison between the C-CCHP and PI-CCHP systems, and analyzed the effects of various operating parameters on system performance. Major assumptions are listed below.

- The system is in a steady state (Wu et al., 2021).
- Stream mixing in the process streams integration module and the HEN is isothermal (Prendl et al., 2021).
- Heat loss and pressure drop in equipment are negligible unless stated otherwise in Section 3.
- Efficiencies of the pumps are fixed (Marandi et al., 2021).
- Hydrogen sent to PEMFC is assumed to be pure (purity = 100%), and composition of air is assumed 21% of oxygen and 79% of nitrogen (Chen et al., 2016).
- Operating temperature and pressure of the PEMFC stack are the same as those of a single fuel cell (Chang et al., 2017b).

3. Mathematical model

In this section, an MINLP model that simultaneously realizes the optimization of heat integration and operating variables for the PI-CCHP system is developed. Subsequently, HEN of the PI-CCHP system is synthesized via an HEN superstructure model based on the optimization results of process streams. Mathematical model of the framework is summarized as **(M1)**. The objective is to maximize energy efficiency of the system (η^{sys}). Symbols and notations are listed in the Nomenclature Section.

(M1)

max η^{sys}

s.t.

MSR module: Eqs. (2)-(10), (S.4)-(S.15)

PEMFC module: Eqs. (11)-(17), (S.16)-(S.38)

PSA module: Eqs. (S.39)-(S.42)

AC module: Eqs. (S.43)-(S.51)

Heat integration module: Eqs. (S.52)-(S.74)

Auxiliaries: Eqs. (S.78)-(S.88)

HEN synthesis model: Eqs. (S.89)-(S.106)

Performance evaluation: Eqs. (18)-(29), (S.107)-(S.122)

3.1. Objective function

Energy efficiency of the system is given by Eq. (1).

$$\eta^{sys} = \frac{W^{net} + Q^{hotw} + Q^{coldw}}{\Delta f^{tot}_{\mathrm{CH_3OH}} \cdot HHV_{\mathrm{CH_3OH}}} \quad (1)$$

where W^{net} is the net power output; Q^{hotw} and Q^{coldw} denote the heating load of hot water and the cooling load of cold water generated from CCHP system, respectively. $\Delta f^{tot}_{\mathrm{CH_3OH}}$ is the total consumption of methanol, and $HHV_{\mathrm{CH_3OH}}$ represents the higher heating value of methanol.

3.2. MSR module

The MSR subsystem is modeled as a reformer, packed with $Cu/ZnO/Al_2O_3$ catalyst particles. Methanol and steam enter the reformer where steam reforming reactions occur to produce hydrogen. This subsection presents the principles of MSR reaction thermodynamics and kinetics and details of the mathematical model of the MSR subsystem. The main chemical reactions carried out in the MSR module can be found in the Supplement Information.

3.2.1. Thermodynamic constraints

Here, modeling of reaction thermodynamics is based on stoichiometric approach. Eq. (2) calculates molar Gibbs free energy ($g_{s,u}$) of substance u in stream s. Molar enthalpy ($mh_{s,u}$) and molar entropy ($ms_{s,u}$) are calculated by Eqs. (3) and (4), respectively.

$$g_{s,u} = mh_{s,u} - ms_{s,u} \cdot T^{MSR} \quad \forall s \in SMSR, u \in UMSR \quad (2)$$

$$mh_{s,u} = \Delta_f h^0_u + \int_{T^{ref}}^{T^{MSR}} CP_{s,u}\, dT \quad \forall s \in SMSR, u \in UMSR \quad (3)$$

$$ms_{s,u} = \Delta_f s^0_u + \int_{T^{ref}}^{T^{MSR}} \frac{CP_{s,u}}{T} dT - R \cdot \ln\left(\frac{p^{MSR}}{p^{ref}}\right) \quad \forall s \in SMSR, u \in UMSR \quad (4)$$

where $SMSR$ and $UMSR$ are the sets of process streams and substances in the MSR subsystem, respectively. $\Delta_f h^0_u$ and $\Delta_f s^0_u$ represent the standard molar enthalpy and entropy of formation, respectively. Moreover, $CP_{s,u}$ is the heat capacity and R stands for the ideal gas constant equal to 8.314 J/(mol·K).

The Gibbs free energy change (Δg^0_m) of reaction m can be obtained by Eq. (5). Eq. (6) reveals the relation between Gibbs free energy change and chemical equilibrium constant (K_m). Eq. (7) defines the chemical equilibrium of reaction m.

$$\Delta g^0_m = \sum_{s \in SMSRO} \sum_{u \in PT} v_{m,u} \cdot g_{s,u} - \sum_{s \in SMSRI} \sum_{u' \in RT} v_{m,u'} \cdot g_{s',u'} \quad \forall m \in RMSR \quad (5)$$

$$\Delta g_m^0 = -R \cdot T^{MSR} \cdot \ln(K_m) \quad \forall m \in RMSR \tag{6}$$

$$K_m = \frac{\prod_{u \in PT} (xcom_u)^{v_{m,u}}}{\prod_{u' \in RT} (xcom_{u'})^{v_{m,u'}}} \quad \forall m \in RMSR \tag{7}$$

where $v_{m,u}$ refers to the stoichiometric number of substance u in reaction m, $RMSR$ is the set of reactions, PT the set of products, RT the set of reactants, $SMSRI$ and $SMSRO$ the sets of inlet and outlet streams of the MSR subsystem, respectively.

3.2.2. Kinetic constraints

The methanol conversion limit can be obtained through thermodynamic model. In practice, however, the reactions occurring in the reformer cannot reach the thermodynamic limit due to the space constraints. Moreover, the size of reformer influences the investment of MSR system significantly. Thus, the reformer is divided into several segments and the reaction rates of each segment are obtained by kinetic analysis. Then, the lengths of each segment can be achieved by the steady-state model equations, so as to optimize the total length of the reformer under a certain methanol conversion rate. Here, the Langmuir-Hinshelwood macro kinetic model is introduced briefly, and the steady-state model equations and supplemental equations of MSR module can be found in the Supplementary Information.

The Langmuir-Hinshelwood macro kinetic model developed and corrected by Peppley et al. (1999) is selected to estimate reaction rate of the MSR process, where Cu/ZnO/Al_2O_3 catalyst is used. Expressions of the reaction rate (r_m) for the three reactions are given as follows:

$$r_{MSR} = \frac{k_{MSR}^{rate} \cdot K^*_{CH_3O(1)} \left(\frac{p_{CH_3OH}}{p_{H_2}^{0.5}}\right)\left(1 - \frac{p_{H_2}^2 p_{CO_2}}{K_{MSR} p_{CH_3OH}}\right) C_{S1}^T C_{S1a}^T S^c \rho^b}{\left[1 + K^*_{CH_3O(1)}\left(\frac{p_{CH_3OH}}{p_{H_2}^{0.5}}\right) + K^*_{HCOO(1)} p_{H_2}^2 p_{CO_2} + K^*_{OH(1)}\left(\frac{p_{H_2O}}{p_{H_2}^{0.5}}\right)\right]\left(1 + K^{0.5}_{H(1a)} p_{H_2}^{0.5}\right)} \tag{8}$$

$$r_D = \frac{k_D^{rate} \cdot K^*_{CH_3O(2)} \left(\frac{p_{CH_3OH}}{p_{H_2}^{0.5}}\right)\left(1 - \frac{p_{H_2}^2 p_{CO}}{K_D p_{CH_3OH}}\right) C_{S2}^T C_{S2a}^T S^c \rho^b}{\left[1 + K^*_{CH_3O(2)}\left(\frac{p_{CH_3OH}}{p_{H_2}^{0.5}}\right) + K^*_{OH(2)}\left(\frac{p_{H_2O}}{p_{H_2}^{0.5}}\right)\right]\left(1 + K^{0.5}_{H(2a)} p_{H_2}^{0.5}\right)} \tag{9}$$

$$r_{WGS} = \frac{k_{WGS}^{rate} \cdot K_{\mathrm{OH}(1)}^{*} \left(\frac{p_{\mathrm{CO}} p_{\mathrm{H_2O}}}{p_{\mathrm{H_2}}^{0.5}}\right)\left(1 - \frac{p_{\mathrm{H_2}} p_{\mathrm{CO_2}}}{K_{WGS} p_{\mathrm{CO}} p_{\mathrm{H_2O}}}\right)\left(C_{S1}^{T}\right)^2 S^c \rho^b}{\left[1 + K_{\mathrm{CH_3O}(1)}^{*}\left(\frac{p_{\mathrm{CH_3OH}}}{p_{\mathrm{H_2}}^{0.5}}\right) + K_{\mathrm{HCOO}(1)}^{*} p_{\mathrm{CO_2}} p_{\mathrm{H_2}}^{0.5} + K_{\mathrm{OH}(1)}^{*}\left(\frac{p_{\mathrm{H_2O}}}{p_{\mathrm{H_2}}^{0.5}}\right)\right]^2} \quad (10)$$

where k_m^{rate} is the rate constant of reaction m. K_u^* refers to the adsorption coefficient of reaction intermediate u, of which the detailed definitions can be found in (Peppley et al., 1997). p_u represents the partial pressure of component u, and C_{S1}^T, C_{S1a}^T, C_{S2}^T and C_{S2a}^T are the total site concentrations of site 1, 1a, 2, and 2a, respectively. S^c represents the surface area per unit mass and ρ^b the density of catalyst.

3.3. PEMFC module

The PEMFC stack model is adopted from (Ahmadi et al., 2016). The PEMFC model formulated in this work is comprised of two parts, namely an electrochemical model and a thermal model.

3.3.1. Electrochemical model of PEMFC

The Nerst potential of single fuel cell ($E^{FC,Nerst}$) consists of the output voltage (V^{FC}), the activation polarization loss ($\Delta V^{FC,act}$), the ohmic polarization loss ($\Delta V^{FC,ohm}$), and the concentration polarization loss ($\Delta V^{FC,conc}$), as defined in Eq. (11).

$$E^{FC,Nerst} = V^{FC} + \Delta V^{FC,act} + \Delta V^{FC,ohm} + \Delta V^{FC,conc} \quad (11)$$

$E^{FC,Nerst}$ can be calculated using Eq (12).

$$E^{FC,Nerst} = 1.229 - 0.8 \times 10^{-3}(T^{FC} - 298.15\ K) + 4.3085 \times 10^{-5} T^{FC} \cdot \ln\left[p_{\mathrm{H_2}}^{e} (p_{\mathrm{O_2}}^{e})^{0.5}\right] \quad (12)$$

where T^{FC} refers to the operating temperature of fuel cell; $p_{\mathrm{H_2}}^e$ and $p_{\mathrm{O_2}}^e$ are the effective partial pressures of hydrogen and oxygen, respectively, which can be calculated using Eqs. (S.16) and (S.17).

Actual voltage of a single fuel cell can be calculated using Eqs. (11), (S.22)-(S.33). Generally, a PEMFC stack includes many single fuel cells, and total power output (W^{FC}) from the stack, therefore, can be obtained by Eq. (13).

$$W^{FC} = n^{FC} \cdot I^{FC} \cdot V^{FC} \quad (13)$$

where n^{FC} denotes the number of single fuel cells in the PEMFC system.

3.3.2. Thermal model of PEMFC

Eq. (14) determines the energy balance of the PEMFC subsystem. The total energy provided by electrochemical reactions ($Q^{tot,FC}$) consists of the net power output, the latent and sensible heat ($Q^{sl,FC}$), and the net heat output ($Q^{net,FC}$).

$$Q^{net,FC} = Q^{tot,FC} - W^{FC} - Q^{sl,FC} \tag{14}$$

The available heat released due to electrochemical reactions is obtained by Eq. (15).

$$Q^{tot,FC} = \Delta f_{\mathrm{H_2}}^{FC} \cdot HHV_{\mathrm{H_2}} \tag{15}$$

where $HHV_{\mathrm{H_2}}$ is the higher heating value of hydrogen.

The latent and sensible heat absorbed can be calculated using Eq. (16).

$$Q^{sl,FC} = \sum_{s \in SFCO} \sum_{u \in UFCO} f_{s,u} \cdot mh_{s,u} - \sum_{s' \in SFCI} \sum_{u' \in UFCI} f_{s',u'} \cdot mh_{s',u'} + \Delta f_{\mathrm{H_2O}}^{FC} \cdot LH_{\mathrm{H_2O}} \tag{16}$$

where $SFCO$ represents the set of outlet streams in fuel cell; $UFCI$ and $UFCO$ refer to the sets of substances at the inlet and outlet of fuel cell, respectively; and $LH_{\mathrm{H_2O}}$ is the latent heat of water.

Eq. (17) calculates the molar enthalpy of each substance in the fuel cell.

$$mh_{s,u} = \int_{T^{ref}}^{T^{FC}} CP_{s,u}\, dT \quad \forall s \in SFC, u \in UFC \tag{17}$$

where SFC and UFC refer to the set of streams and substances in fuel cell, respectively.

3.4. Performance evaluation

3.4.1. Thermodynamic performance model

Net power output of the distributed generation system can be expressed as Eq. (18). In addition, the heating output of hot water and cooling output of cold water produced by trigeneration are calculated using Eqs. (19) and (20), respectively. It should be pointed out that only the heat content above 313.15 K for hot water is taken into account as heating output, as stated in Eq. (19).

$$W^{net} = W^{FC} - W^{rfp} - W^{CT} - \sum_{e \in EACP} W_e - \sum_{e \in EWP} W_e \tag{18}$$

$$Q^{hotw} = 4.2 \times 10^3 m^{hotw} \left(T^{hotw,out} - 313.15\ K\right) \tag{19}$$

$$Q^{coldw} = Q_e \quad \forall e \in EACEVA \tag{20}$$

Eq. (21) defines the power generation efficiency of the system (η^{ele}).

$$\eta^{ele} = \frac{W^{net}}{\Delta f^{tot}_{\mathrm{CH_3OH}} \cdot HHV_{\mathrm{CH_3OH}}} \tag{21}$$

Eq. (22) states that the exergy efficiency of the trigeneration system ($\eta^{ex,sys}$) is a ratio of the sum of net power output, hot water (Ex^{hotw}) and chilling water's exergy (Ex^{coldw}) to the chemical exergy of methanol ($Ex_{\mathrm{CH_3OH}}$).

$$\eta^{ex,sys} = \frac{W^{net} + Ex^{hotw} + Ex^{coldw}}{Ex_{\mathrm{CH_3OH}}} \tag{22}$$

Here, Ex^{hotw}, Ex^{coldw} and $Ex_{\mathrm{CH_3OH}}$ can be obtained by Eqs (23)-(25), respectively.

$$Ex^{hotw} = Q^{hotw}\left(\frac{T^{hotw,out} - T^{amb}}{T^{hotw,out}}\right) \tag{23}$$

$$Ex^{coldw} = Q^{coldw}\left(\frac{T^{amb} - T^{coldw,out}}{T^{coldw,out}}\right) \tag{24}$$

$$Ex_{\mathrm{CH_3OH}} = \Delta f^{tot}_{\mathrm{CH_3OH}} \cdot ex_{\mathrm{CH_3OH}} \tag{25}$$

where $ex_{\mathrm{CH_3OH}}$ is chemical exergy of 1 mol methanol under standard condition.

3.4.2. Economic performance model

Levelized cost of electricity ($LCOE$) is selected to evaluate the economic performance of the distributed generation system. Expression of $LCOE$ is given in Eq. (26), and it can be considered as the lowest price at which (equivalent) electricity should be sold to pay off the total cost of the system over its lifetime. Here, the numerator represents equivalent annual cost of the distributed generation system. The denominator is the equivalent electricity generated by the system, where heating and cooling produced are converted into equivalent electrical energy.

$$LCOE = \frac{CRF \cdot C^{tot,inv} + C^{opr} + C^{fuel}}{\left(W^{net} + \frac{Q^{hotw}}{4} + \frac{Q^{coldw}}{3}\right) t^{opr}} \tag{26}$$

where CRF denotes the capital recovery rate; $C^{tot,inv}$, C^{opr}, and C^{fuel} are total investment, annual operating cost, and annual fuel cost of trigeneration system, respectively, as defined by Eqs. (27)-(29) . In addition, t^{opr} is the annual operation time. Cost functions for each item of equipment are listed in detail in Table S7.

$$C^{tot,inv} = \sum_{e \in ECCHP} C_e^{inv} \tag{27}$$

$$C^{opr} = 0.06C^{tot,inv} \tag{28}$$

$$C^{fuel} = t^{opr}\left(UC_{\mathrm{CH_3OH}}\Delta f^{tot}_{\mathrm{CH_3OH}} + UC_{\mathrm{H_2O}}\Delta f^{tot}_{\mathrm{H_2O}}\right) \tag{29}$$

where $ECCHP$ is the set of subsystems in trigeneration system; $UC_{\mathrm{CH_3OH}}$ and $UC_{\mathrm{H_2O}}$ represent the unit costs of methanol and water, respectively.

3.5. Model validation

We verify the proposed model by measuring the performance of main subsystems, which include the MSR system, the PEMFC stack and the AC system, against the results reported in the literature (Florides et al., 2003; Peppley et al., 1999; Ahmadi et al., 2016). As shown in Fig. 3 (a) and (b), the simulation results are in good agreement with the reference results. The mean relative error of methanol conversion rate is 1.14% for the MSR system and that of the actual voltage is 0.83% for the PEMFC stack. Moreover, the model validation for the AC system proves that the AC system model is accurate enough as its maximum relative error is 0.15%.

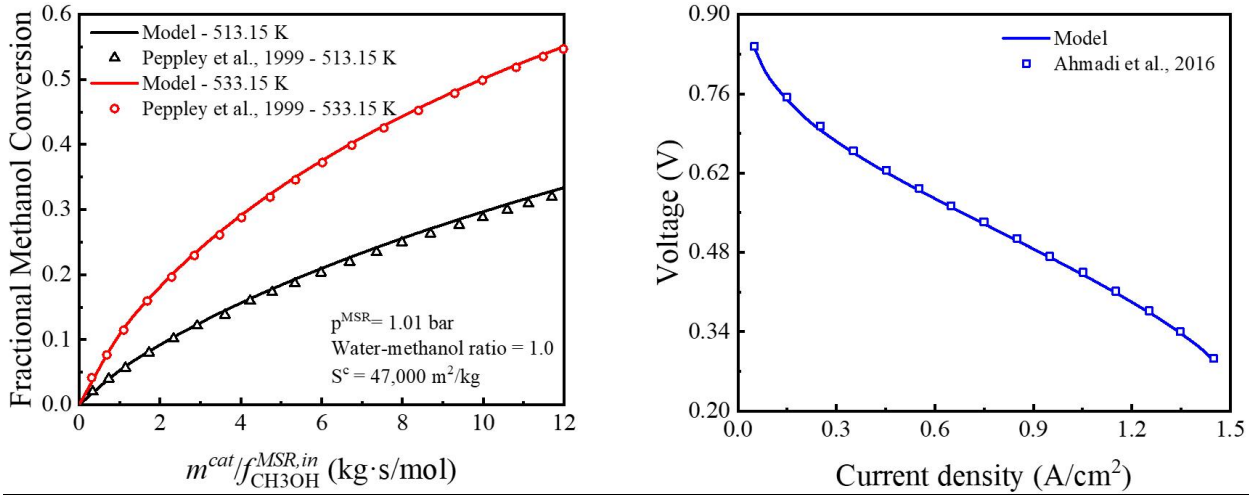

(a) (b)

Fig. 3 Model validation for (a) Methanol conversion rate of the MSR system and (b) Polarization curve of single fuel cell.

Table 1 Model validation for the AC system (Florides et al., 2003)

Items	Model	(Florides et al., 2003)	Relative error
Heating load of evaporator (kW)	10.00 (Input)	10.00 (Input)	/
Heating load of absorber (kW)	13.42	13.44	0.15%
Heating load of generator (kW)	14.20	14.22	0.14%
Heating load of condenser (kW)	10.78	10.78	≈ 0
Power consumption of pump (kW)	0.29	0.29	≈ 0
Coefficient of performance	0.70	0.70	≈ 0

4. Optimization strategy

The model presented in Section 3 includes large number of continuous variables (e.g. operating temperature and pressure, molar flow rate of reactants and products), binary variables (e.g. discrete decision variables in the heat integration model) and nonlinear constraints (e.g. reaction equilibriums), making it difficult to be solved directly by off-the-shelf solvers. In this section, a two-step method is introduced to tackle the challenges so as to achieve optimization and HEN synthesis for the cogeneration system.

Fig. 4 presents the procedure of the two-step algorithm. Step 1 focuses on identifying the optimal design of the system with consideration of heat integration. In this step, we first search for a feasible solution for MSR, PEMFC and AC subsystems. Then, feasible solutions for each subsystem are input as initial values to the next stage to achieve a local optimal solution for the distributed generation system. Next, the local solution is used as a starting point for global solver to find the global optimal solution. Based on the results of process streams obtained in the first step, Step 2 synthesizes the optimal HEN using the superstructure method (Liang et al., 2022b). It should be noted that each stage often requires multiple iterations to update the initial values and bounds to alleviate the solution difficulty due to the nonconvexity of the model. A detailed flowchart of the algorithm is available in the Supplementary Information in Fig. S2.

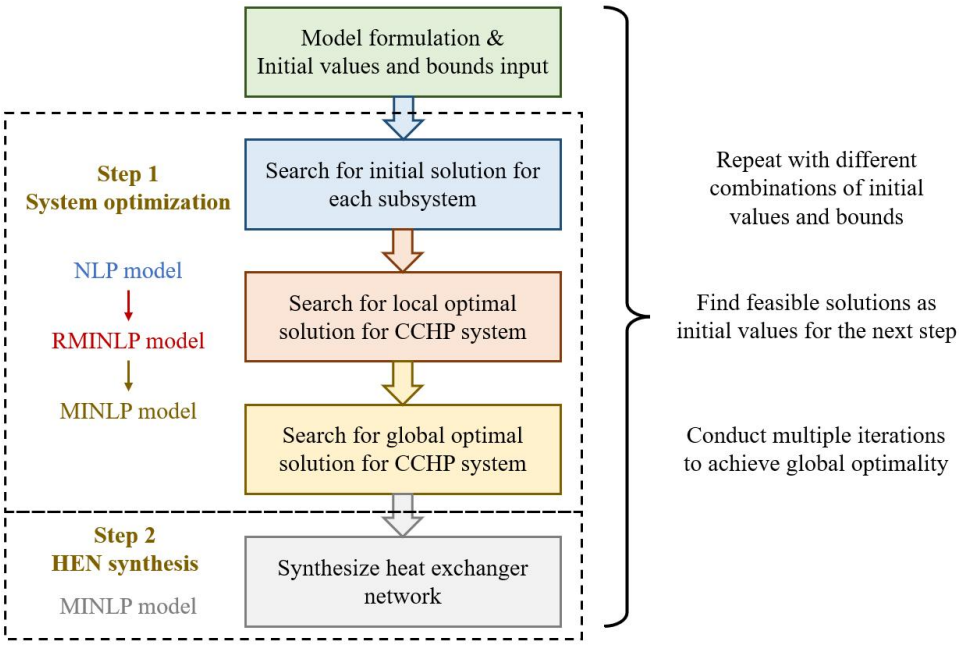

Fig. 4 Procedure of the two-step optimization method.

5. Results and discussion

In this section, a numerical study of a 1,000-kWe scale PI-CCHP system is first carried out with the objective to determine the optimal design for a methanol-reforming PEMFC-based distributed generation system. Next, we present a comparison between the C-CCHP system and the PI-CCHP system to demonstrate the effectiveness of our proposed integrated design and optimization method. Finally, we conduct a sensitivity analysis of the PI-CCHP system to evaluate the impact of design parameters on the cooling, heating, power-generation performance, and economics of the system.

5.1. System optimization

Subsection 5.1 presents the system optimization of a 1,000-kWe scale PI-CCHP system with the objective of improving energy efficiency. The design parameters of this case study are listed in Table 2, and the effectiveness of the optimization method is validated. The results show that a PI-CCHP system with high energy efficiency can be obtained through the proposed optimization method. Key operating conditions, such as the reaction temperature of the MSR subsystem, operating pressure and temperature in the PEMFC, are design variables to be optimized. Table 3 gives the boundary of key design variables. The PI-CCHP system model has

5,005 variables and 5,552 constraints. It takes 477.72 CPUs in total to optimize the PI-CCHP system with a relative optimality tolerance of 10^{-6}.

Table 2 Given design parameters of PI-CCHP system.

Items	Values	Ref.
Ambient temperature (T^{amb})	298.15 K	(Wang et al., 2017)
Isentropic efficiency of pump (η^{pump})	87%	(Chen et al., 2020)
Minimum approach temperature in HEN (ΔT^{MIN})	10 K	(Loreti et al., 2019)
Power demand	1,000 kW	/
Reaction pressure of MSR (p^{MSR})	1,500 kPa	(Wang et al., 2017)
Water-methanol ratio	1	(Wang et al., 2017)

Table 3 Boundary of key design variables. *

Variables	Boundaries	Ref.
Reaction temperature of MSR (T^{MSR})	473.15-573.15 K	(Wang et al., 2017)
Operating temperature of PEMFC (T^{FC})	358.15-368.15 K	(Chen et al., 2015)
Operating pressure of PEMFC (p^{FC})	100-400 kPa	(Mert et al., 2007)
Current density (i^{FC})	0-150 A/m^2	(Ahmadi et al., 2016)
Molar flow rate of stream ($f_{s,u}$)	0-10,000 mol/s	/
Inlet temperature of heat integration module	298.15-593.15 K	/
Outlet temperature of heat integration module	298.15-593.15 K	/

*Reaction temperature of MSR and operating condition of PEMFC are to be optimized.

Table 4 lists the optimal operating conditions of the PI-CCHP system. The results report a maximum overall energy efficiency of 88.50% for the proposed PI-CCHP system. It can be seen that the reaction temperature in MSR has reached the upper bound, which can be explained by Le Chatelier's principle. According to Eqs. (S.1)-(S.3), a higher reaction temperature is beneficial to the endothermic methanol-steam reforming reaction. In addition, the operating pressure of PEMFC tends to be close to the lower bound while the operating temperature inclines to its upper bound. The reasoning will be presented later in discussion of Fig. 11.

Table 4 Optimal operating conditions/performance of the PI-CCHP system.

Items	Values
System energy efficiency	88.50%
System exergy efficiency	20.81%
Gross power output (including power consumption of the pumps)	1,024.03 kW
Heating load of hot water	1,578.10 kW
Cooling load of cold water	2,811.10 kW
$LCOE$	0.2374 $/kWh
Hot utility	343.27 kW
Cold utility	131.10 kW
Reaction temperature of MSR	573.15 K
Operating temperature of PEMFC	365.92 K
Operating pressure of PEMFC	119 kPa

Composite curve of the PI-CCHP system is shown in Fig. 5. After heat integration, the minimum hot utility and cold utility of the system are 343.27 kW and 131.10 kW, respectively. The pinch occurs at 320.73 K/310.73 K, and the cold streams recover a total 772.84 kW of thermal energy from the hot streams. Since the temperature and the heat capacity flow rate of each stream have been determined in Step 1, the corresponding HEN can now be obtained by the superstructure method in Step 2 of the proposed algorithm. The optimal HEN design of the PI-CCHP system is shown in Fig. 6 with 12 heat exchangers, 2 heaters, and 4 coolers.

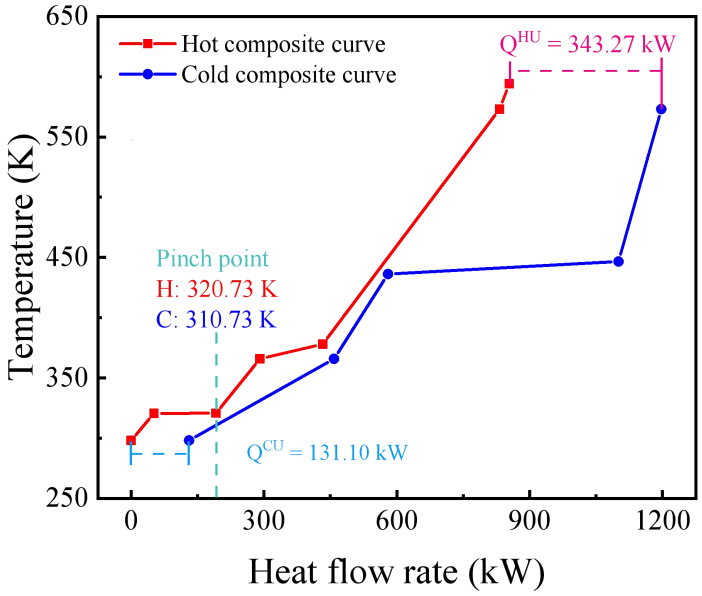

Fig. 5 Composite curves of a 1,000 kWe scale PI-CCHP system.

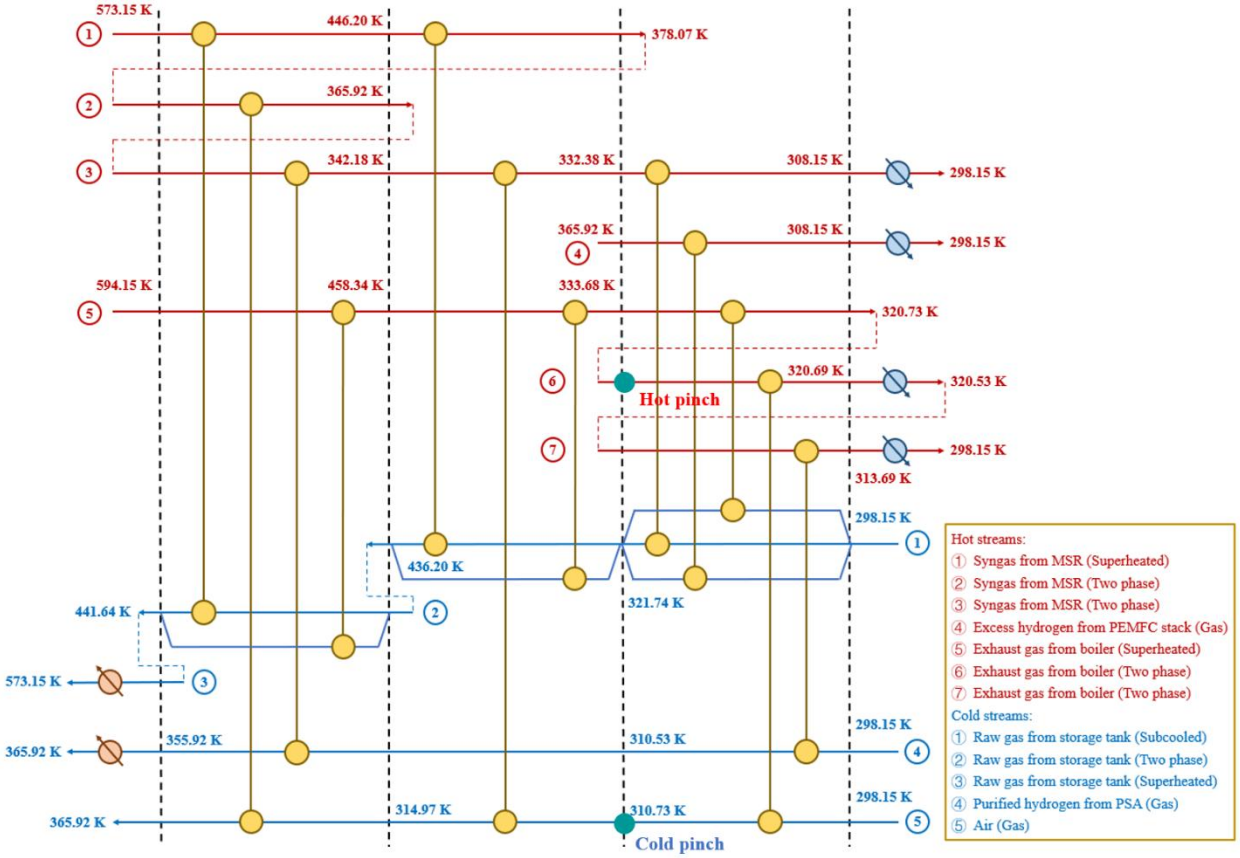

Fig. 6 HEN configuration of a 1,000 kWe scale PI-CCHP system.

5.2. Comparison with conventional CCHP system

The optimization in Subsection 5.1 has demonstrated the optimization and design procedures of the PI-CCHP system. In this subsection, the comparison results between different CCHP system designs are presented in detail to illustrate the advantages of the proposed PI-CCHP system. Table 5 lists the given design parameters of MSR and PEMFC systems, and other design parameters are the same as those in Table 2. In order to compare the PI-CCHP and C-CCHP systems, we have adopted a baseline approach by fixing the operating temperature and pressure of Proton Exchange Membrane Fuel Cells (PEMFC) and the reaction temperature of Molten Salt Reactors (MSR). This approach is distinct from our previous optimization study. The baseline parameters are taken from relevant literature sources, and are used as a reference point for evaluating the performance of both systems. The aim of this approach is to provide a reliable and objective comparison between the PI-CCHP and C-CCHP systems.

Table 5 Given design parameters of CCHP systems in the comparison study. *

Items	Values	Ref.
Operating temperature of PEMFC (T^{FC})	363.15 K	(Chen et al., 2015)
Operating pressure of PEMFC (p^{FC})	200 kPa	(Chen et al., 2015)
Reaction temperature of MSR (T^{MSR})	523.15 K	(Wang et al., 2017)

*Operating conditions of MSR and PEMFC are fixed.

Table 6 gives the operating conditions and comprehensive performances of the two CCHP systems. Due to the fixed PEMFC and MSR design variables, the energy efficiency of the PI-CCHP system drops 3.37 percentage point compared with the design obtained in previous subsection. However, the PI-CCHP system still manages to achieve a 6.38% decrease in methanol consumption compared with the C-CCHP system. This is likely due to the effective heat integration that improves the energy efficiency of the system, and less methanol is required as fuel to compensate for the heat deficit. Overall, the PI-CCHP system achieves 5.45, 1.99 and 2.22 percentage points increases in energy efficiency, net electrical efficiency and exergy efficiency, respectively. It can be attributed to the significant reduction in hot utility. In addition, the PI-CCHP system shows a better economic performance, with a 4.95% decrease in the $LCOE$ in contrast to the C-CCHP system.

437 Table 6 Operating conditions and comprehensive performances of different CCHP systems.

Items	C-CCHP	PI-CCHP
Operating temperature of PEMFC (T^{FC})	363.15 K	363.15 K
Operating pressure of PEMFC (p^{FC})	200 kPa	200 kPa
Reaction temperature of MSR (T^{MSR})	523.15 K	523.15 K
Reaction pressure of MSR (p^{MSR})	1,500 kPa	1,500 kPa
Methanol consumption	4.70 mol/s	4.40 mol/s
Gross power output (including power consumption of the pumps)	1,009.31 kW	1,009.66 kW
Heating load of hot water	623.70 kW	624.12 kW
Cooling load of cold water	1,096.88 kW	1,097.62 kW
Hot utility	387.32 kW	209.78 kW
Cold utility	27.35 kW	84.03 kW
Energy efficiency (η^{sys})	79.68%	85.13%
Net electricity efficiency (η^{ele})	29.29%	31.28%
Exergy efficiency ($\eta^{ex,sys}$)	32.65%	34.87%
Levelized cost of electricity ($LCOE$)	0.2182 $/kWh	0.2079 $/kWh

438

439 Fig. 7 compares the composite curves of the two CCHP systems. It can be noted that the hot
440 utility and cold utility of the C-CCHP system are 282.44 kW and 26.67 kW, respectively. A
441 notable reduction in hot utility to 209.78 kW can be achieved for the PI-CCHP system by the aid
442 of the heat integration that allows heat exchange among all streams. On the other hand, we notice
443 that cold utility of the PI-CCHP system increases to 84.03 kW due to the introduction of other
444 hot streams such as tail gas. However, since the unit cost of cold utility is significantly lower
445 than that of hot utility, the heat integration of the PI-CCHP system is not only energetically
446 advantageous, but also economically viable.

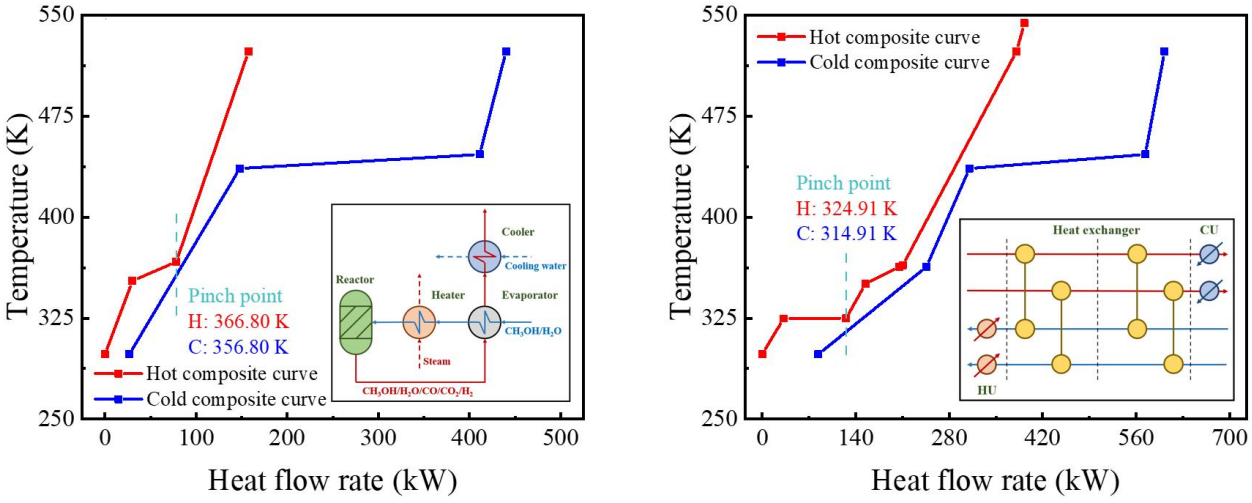

(a) (b)

Fig. 7 Composite curves of (a) C-CCHP system and (b) PI-CCHP system.

Fig. 8 shows the cost distribution of the two CCHP systems. We can see from Fig. 8(a), while the initial investment of the PI-CCHP system is about 1.8% higher, the integrated design is more economically advantageous in the long run with an $LCOE$ of 0.2090 \$/kWh, 4.5% lower than that of the C-CCHP system. The cost reduction is mainly due to the decrease in raw material cost (mostly from methanol), which is the major contributor to the equivalent annual cost of the system. In terms of the initial investment, Fig. 8(b) and Fig. 8(c) show that the two systems share similar investment distribution in PEMFC, PSA and absorption cooling subsystem, among which the PEMFC and the PSA are much more expensive items, taking up over 58% and 28% of the total investment, respectively. Fig. 8(d) gives details of the investment in other equipment. We notice that, as a result of the lower hot utility demand, the PI-CCHP system cuts down its boiler cost by 19.61% compared with the C-CCHP system. The investment in methanol storage tank in the PI-CCHP system is also reduced by 3.4% due to its lower methanol consumption. Furthermore, it is worthwhile to note that, the investment in heat exchanger of the PI-CCHP system is higher than that of the C-CCHP system by \$70,194. However, the difference in HEN investment is negligible as it only accounts for 2.03% of the total investment cost of the PI-CCHP system and annualized investment cost is a fraction compared with material (methanol) cost. As such, it is reasonable to apply the two-step method to find the optimal energy target of the system by simultaneous heat integration and process optimization, then synthesize the HEN.

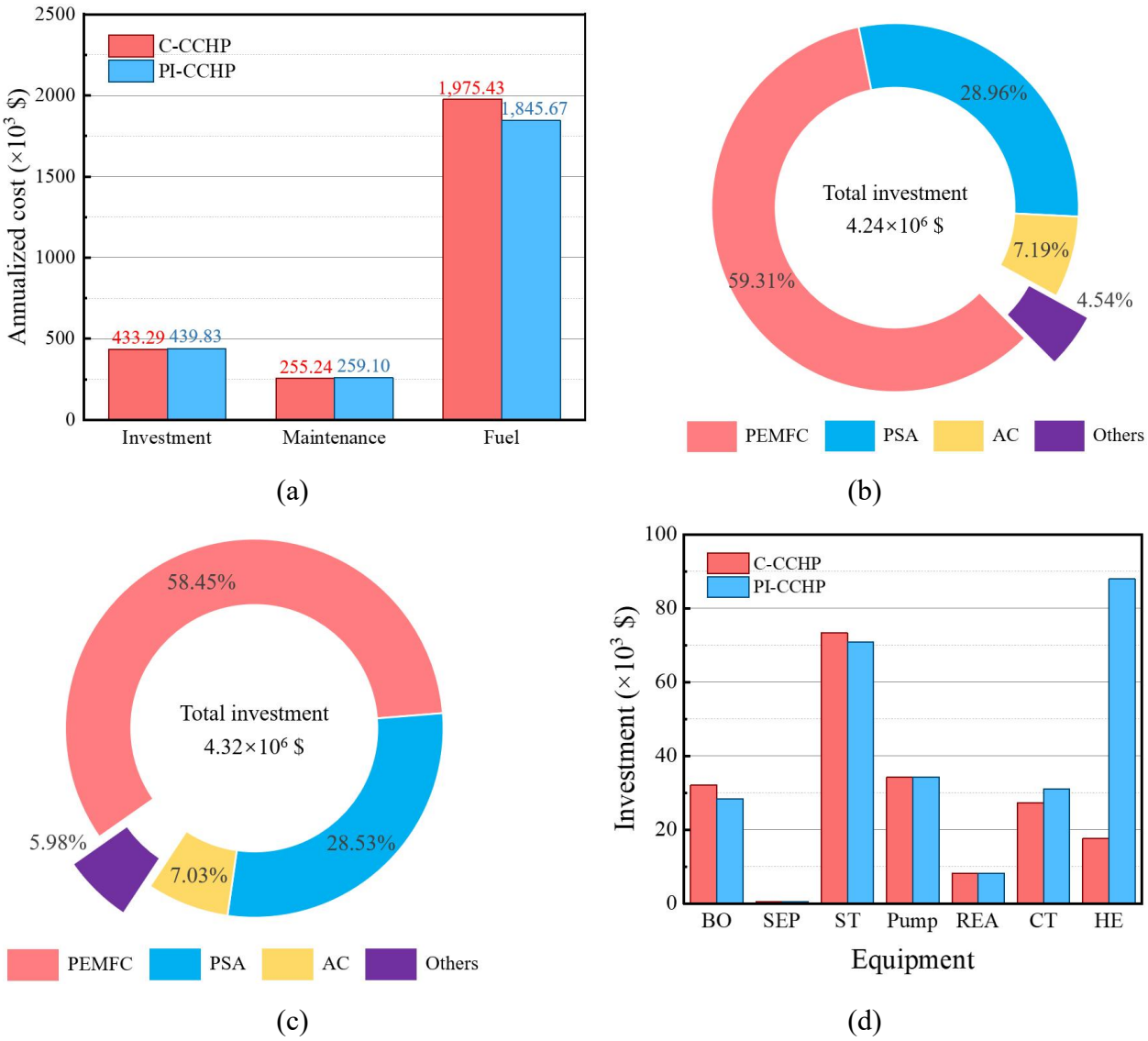

Fig. 8 Economic performances of the CCHP systems: (a) Annual cost of the CCHP systems, (b) Investment breakdown of the CCHP system, (c) Investment breakdown of the PI-CCHP system and (d) Investment breakdown of other equipment.

In addition, the PI-CCHP system is also compared with similar system in the literature. Table 7 displays the comparison results. The energy efficiency of PI-CCHP system is 28.40% and 6.13% higher than that of the CCHP systems in (Chen et al., 2020) and (Ge et al., 2023) respectively. However, the exergy efficiency of PI-CCHP system is relatively low due to the high heating-electricity and cooling-electricity ratios. It means that more chemical energy of methanol is converted into the heat rather than the electricity in the PI-CCHP system under the energy objective.

480 Table 7 Comparison results between the PI-CCHP system and similar system in the literature.

Items	(Chen et al., 2020)	(Ge et al., 2023)	PI-CCHP
Operating temperature of PEMFC (T^{FC})	358.15 K	343.15 K	363.15 K
Operating pressure of PEMFC (p^{FC})	101 kPa	203 kPa	200 kPa
Reaction temperature of MSR (T^{MSR})	473.15 K	523.15 K	523.15 K
Reaction pressure of MSR (p^{MSR})	101 kPa	101 kPa	1,500 kPa
Methanol consumption	0.035 mol/s	0.167 mol/s	4.401 mol/s
Natural gas flow rate	/	0.618 mol/s	/
Net power output (W^{net})	7.09 kW	228.89 kW	1,000 kW
Heating load of hot water (Q^{hotw})	12.22 kW	181.53 kW	624.12 kW
Cooling load of cold water (Q^{coldw})	3.73 kW	47.40 kW	1097.62 kW
Energy efficiency (η^{sys})	66.30%	80.21%	85.13%
Net electricity efficiency (η^{ele})	20.40%	33.73%	31.28%
Exergy efficiency ($\eta^{ex,sys}$)	47.24%	41.71%	34.87%

481

482 ## 5.3. Sensitivity analysis

483 In this subsection, we investigate the influence of operating parameters of the MSR system
484 and the PEMFC stack on performance of the PI-CCHP system in different energy-generation
485 scenarios. Table 8 gives the inputs of design parameters, while the other parameters remain the
486 same as listed in Table 2.

487 Table 8 Inputs of design parameter for the sensitivity analysis.

Subsystems	Items	Values
MSR system	Reaction temperature of MSR	473.15-573.15 K
	Water-methanol ratio of MSR	1-2
	Operating temperature of PEMFC	363.15 K
	Operating pressure of PEMFC	200 kPa
PEMFC stack	Reaction temperature of MSR	533.15 K
	Water-methanol ratio of MSR	1
	Operating temperature	358.15-368.15 K
	Operating pressure	100-400 kPa

Fig. 9 displays the thermodynamic performance of the PI-CCHP system with different methanol-water ratio as a function of the reaction temperature of MSR. It is evident that a smaller water-methanol ratio is more favorable in terms of the energy and exergy performances, as the system achieves an energy and an exergy efficiency of about 85% and 35%, respectively, when the ratio is equal to 1; while the efficiencies decline to about 81% (energy) and 33% (exergy) when the ratio is increased to 2. On the other hand, the thermodynamic performance is in general insensitive to the reaction temperature for the investigated range. Although one may argue that it is counter-intuitive to reduce the water-methanol ratio since excessive water increases the conversion rate of methanol and production of hydrogen, it does not necessarily improve the overall energy/exergy efficiency. This is because the vaporization process of water absorbs large amount of heat, and increasing the amount of water will lead to greater heat demand. Moreover, as illustrated in Fig. 7, the reactant (the flat blue curve at the top) is not an ideal heat sink to recover latent heat from the effluent for it contains greater amount of water and methanol, and a minimum heat recovery temperature difference is required. Thus, greater consumption of hot utility, i.e. more methanol as fuel for heat, is necessary to satisfy the heat demand. In sum, balancing the methanol-water ratio is crucial for optimizing the thermodynamic performance of the PI-CCHP system. In addition, further discussion on the water-methanol ratio is given in the Supplementary Information.

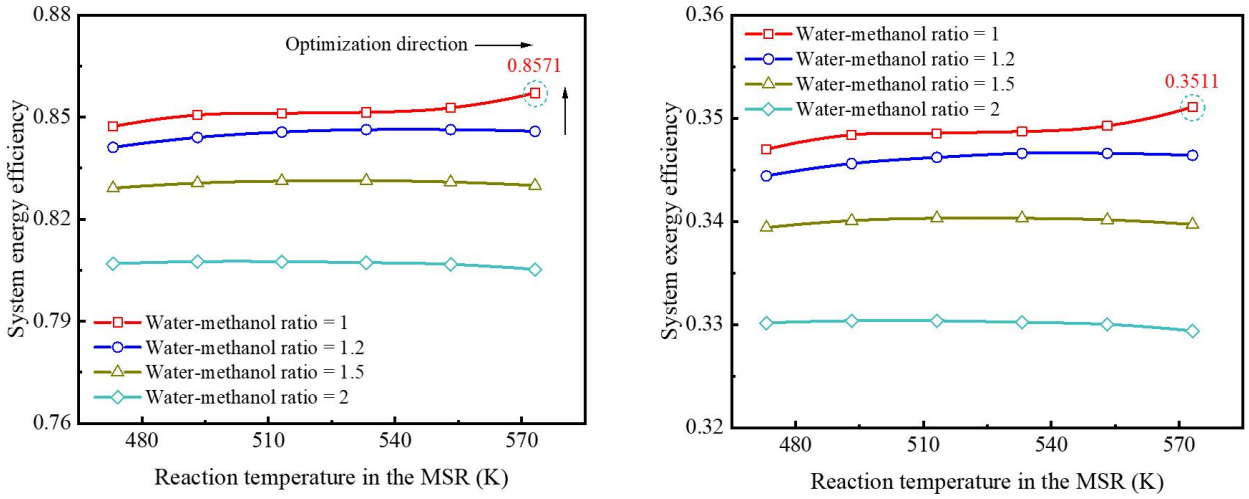

(a) (b)

Fig. 9 Thermodynamic performances of the PI-CCHP system at different MSR reaction temperatures: (a) Energy efficiency and (b) Exergy efficiency.

Furthermore, the insensitivity of energy/exergy efficiency to the reaction temperature is likely due to the tradeoff between the conversion ratio of methanol and the selectivity of the reactions. As can be seen from Fig. 10, the escalation in CO production suggests that the temperature increase is more favorable to the methanol decomposition reaction (Eq. (S.2)), leading to greater methanol consumption as a result. At the same time, because the integrated design allows recovery of tail gas of CO from PSA as fuel to the boiler, less methanol is utilized for burning. Consequently, the total consumption of methanol and energy/exergy efficiency remain mostly unchanged. With the consideration of manageable reaction conditions, it is recommended to maintain a relative low reaction temperature for the MSR subsystem.

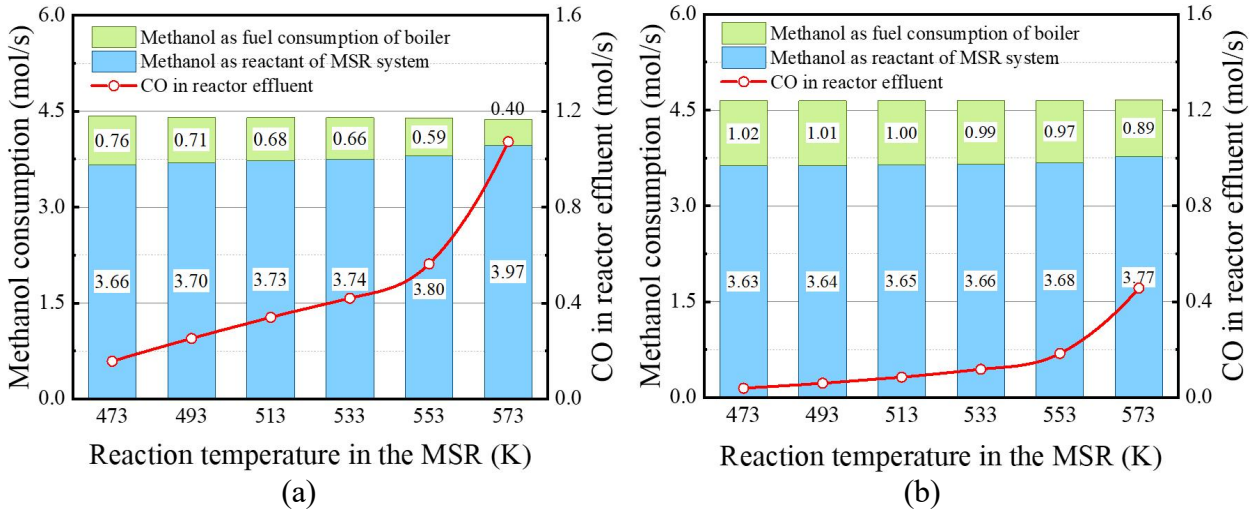

Fig. 10 Methanol consumption and carbon monoxide production at different reaction temperatures of the MSR system: (a) Water-methanol ratio = 1 and (b) Water-methanol ratio = 2.

Fig. 11 shows the energy efficiency of the PI-CCHP system at different PEMFC operating temperatures/pressures. As the operating pressure is increased from 100 kPa to 400 kPa, the system energy efficiency gradually declines. The results can be explained by Fig. 12 and Fig. 13. The energy output of PEMFC consists of net power output and net heat output. A higher operating pressure means a higher actual voltage of a single fuel cell, leading to a higher electricity efficiency of PEMFC. Correspondingly, the heat recovered and utilized by the AC system decreases. Therefore, the heating and cooling loads generated by the AC system are also reduced when the PEMFC operates at higher pressure. A maximum system energy efficiency of 87.14% is obtained at an operating temperature of 368.15 K and under a pressure of 100 kPa. Moreover, we can see that the PI-CCHP system with a higher operating temperature of PEMFC

achieves a greater system energy efficiency under an operating pressure of lower than 150 kPa. Therefore, lowering the temperature of PEMFC is more suitable for the PI-CCHP system when the operating pressure exceeds 150 kPa. For instance, the PEMFC system at 368.15 K/400 kPa achieves the lowest PI-CCHP system energy efficiency of 83.95%, 0.36% lower than the one at 358.15 K/400 kPa. Furthermore, it is also illustrated that a PEMFC system with a lower operating pressure and a higher operating temperature is beneficial to the improvement in the PI-CCHP system efficiency. In addition, it is observed that the influence of operating temperature on the energy efficiency varies depending on the operating pressure, which can be attributed to the effects of the Nernst potential, activation loss, and effective partial pressure of reactant in the PEMFC. This phenomenon is illustrated in detail in Fig. 13.

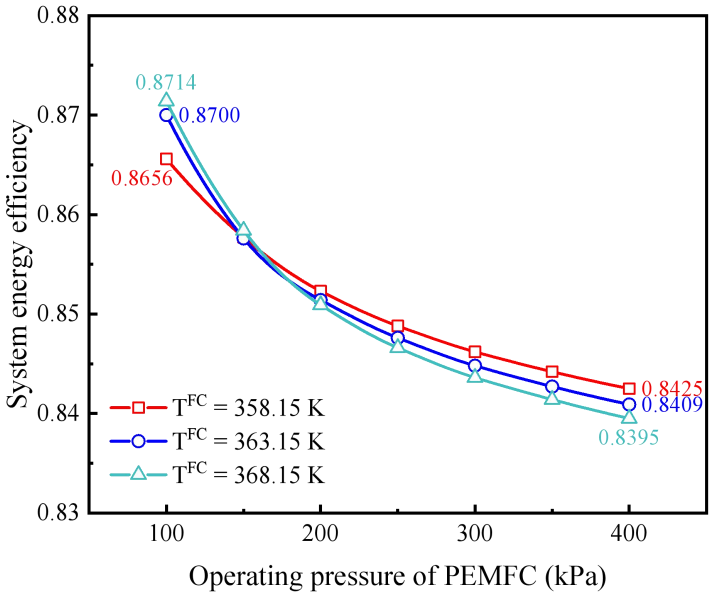

Fig. 11 System energy efficiency at different operating conditions of PEMFC.

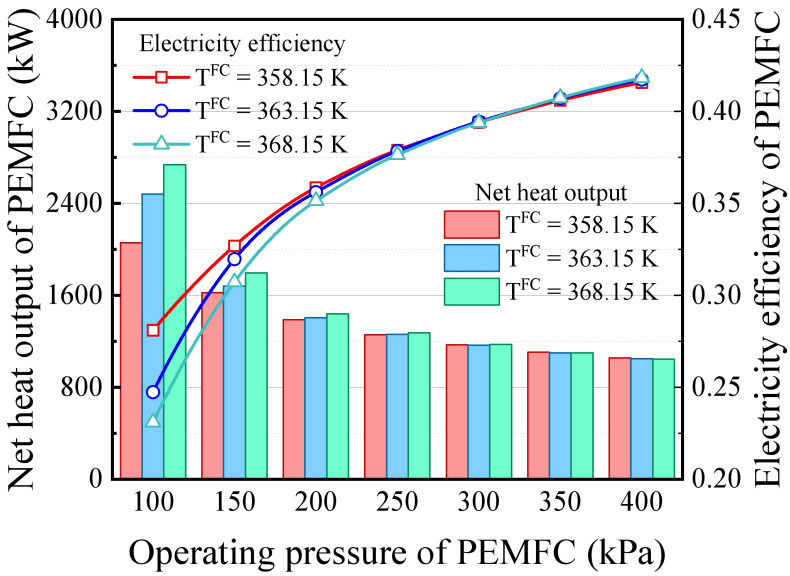

Fig. 12 Net heat output and electricity efficiency at different operating conditions of PEMFC

Fig. 13(a) shows that at low operating pressures, a lower operating temperature leads to a higher actual voltage in the PEMFC, as per the electrochemical model of PEMFC outlined in section 3.3.1. This phenomenon is attributed to the decline in Nernst potential with an increase in operating temperature. The chemical to electrical energy conversion efficiency is also higher in the PEMFC with lower temperature compared to higher temperatures. However, as the operating pressure increases, the difference in actual voltage between the two temperatures diminishes. This trend is due to the significant decline in activation loss with an increase in operating pressure in the PEMFC with higher operating temperature (Fig. 13(b)).

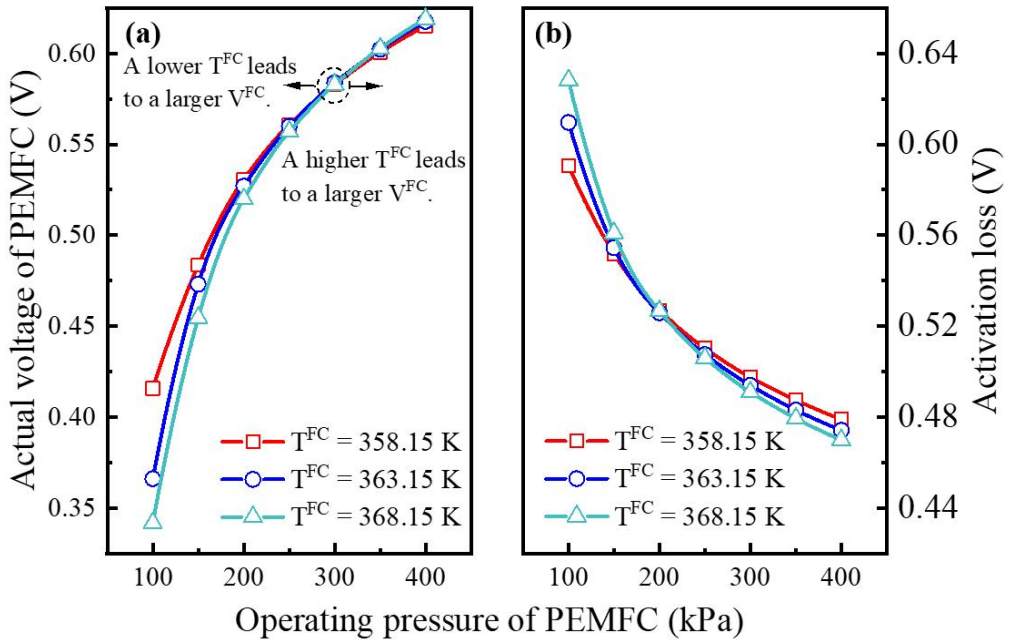

Fig. 13 Operating characteristics of a single fuel cell in the PEMFC stack: (a) Actual voltage and (b) Activation loss.

Fig. 14 illustrates distributions of energy output of the PI-CCHP system at different PEMFC operating conditions. We notice the heating load of hot water and the cooling load of chilled water decrease steadily with the increase of PEMFC operating pressure, as can be seen in Fig. 14(a) and Fig. 14(b). The opposite is true when the PEMFC operating temperature increases. That is, a higher operating temperature leads to a larger heating load, but the margin of improvement is reduced gradually as the operating pressure increases. The PI-CCHP system with a higher operating temperature of PEMFC achieves a larger cooling load of chilled water under an operating pressure of lower than 300 kPa. The results show that the largest heating load is 1,207.30 kW and the cooling load is 2,138.96 kW when the operating condition of PEMFC is 368.15 K/100 kPa. Furthermore, the pattern of variation in methanol consumption is similar to those of heating load and cooling load along with the change of PEMFC operating conditions. However, higher methanol consumption also leads to lower system exergy efficiency. Specifically, the operating conditions that result in the highest system efficiency also lead to the lowest exergy efficiency of 24.23%, mainly because more chemical energy from methanol is converted into heating and cooling load instead of electricity.

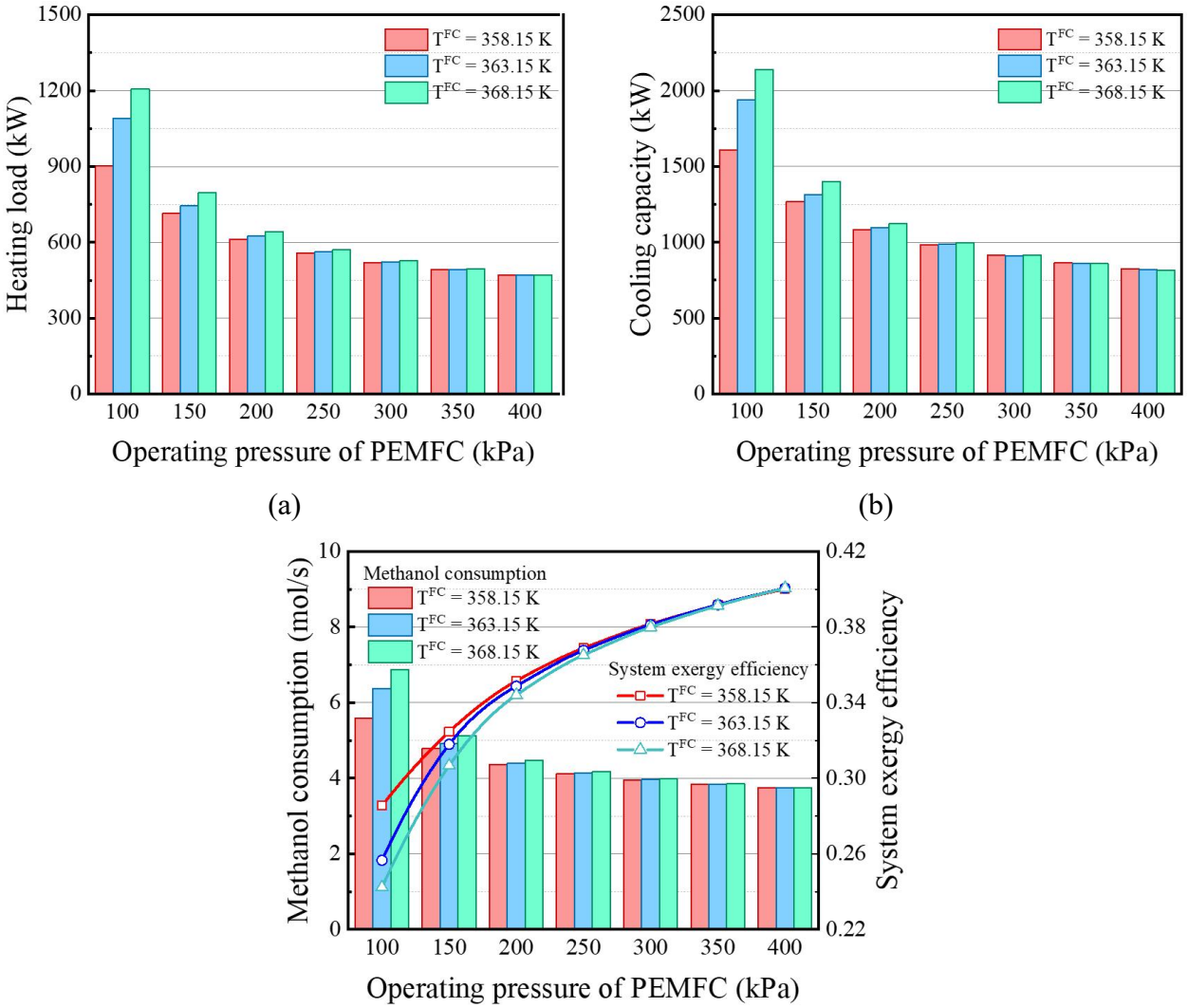

Fig. 14 Thermodynamic performances of PI-CCHP under different operating conditions of PEMFC: (a) Heating load, (b) Cooling capacity and (c) Methanol consumption and exergy efficiency.

6. Conclusion

An equation-oriented framework has been presented for the optimization of combined cooling, heating and power system based on the methanol-steam-reforming proton exchange membrane fuel cell. The framework incorporates kinetics/thermodynamics of unit operations, equation of state, energy targeting and system economics so that it allows simultaneous heat integration and flowsheet optimization. The model has been proved to be accurate and computationally efficient, and its application to the optimization of a 1,000-kWe distributed

generation system has shed some light on the integrated design of methanol-steam-reforming and proton exchange membrane fuel cell for trigeneration from a systematic perspective. In addition, the framework is designed to be modular, allowing for easier extension to other configurations of combined cooling, heating and power system. Major findings are summarized as follows.

- In general, the combined cooling, heating and power system with process integration is thermodynamically and economically beneficial to heat recovery. The proposed system achieves a maximum η^{sys} of 85.13% and maximum $\eta^{ex,\,sys}$ of 34.87%, making a 5.45 percentage point increase in η^{sys} and a 2.22 percentage point increase in $\eta^{ex,\,sys}$, compared with the conventional combined cooling, heating and power system.
- Economic evaluation shows that the combined cooling, heating and power system with process integration obtains a levelized cost of electricity of 0.2374 $/kWh, 4.50% lower than that of the conventional combined cooling, heating and power system. In addition, the results show that the heat exchanger network cost only takes up a small fraction (2.03%) of the total investment, suggesting that the two-step method for sequential system optimization and heat exchanger network synthesis is reasonable and effective in reducing computational complexity.
- Though counter-intuitive, the optimization study and sensitivity analysis of the combined cooling, heating and power system with process integration demonstrate that lowering the water-methanol ratio of methanol steam reforming system facilitates the increase of overall η^{sys} and $\eta^{ex,\,sys}$ within the assessed range. While increasing water-methanol ratio is beneficial to the conversion of methanol in a local point of view for the methanol steam reforming subsystem, from a systematic perspective it will lead to greater energy consumption for reactant heating and lower energy efficiency.
- Further, while the optimization study shows that a higher reaction temperature is beneficial to the combined cooling, heating and power system with process integration in terms of energy efficiency, sensitivity analysis suggests a different picture that the overall η^{sys} and $\eta^{ex,\,sys}$ are not very sensitive to the temperature due to the tradeoff between conversion and selectivity of methanol steam reforming reactions. Generally speaking, it is more favorable to maintain a lower methanol steam reforming temperature for manageable reaction condition as reaction temperature in the range of 473.15-573.15 K has marginal effects on energy/exergy efficiency.

Finally, the proposed combined cooling, heating, and power system, which solely uses methanol as an energy input, leads to higher fuel costs. Additionally, optimizing the system design and operation based only on energy objectives maybe uneconomical. To address these issues, we plan to propose a renewable energy assisted combined cooling, heating, and power system that utilizes the methanol-steam-reforming proton exchange membrane fuel cell. In the future, a multi-objective assessment considering energy, economic, and environmental targets will be conducted. Moreover, we plan to analyze the dynamic characteristics of the system to develop an appropriate control strategy for improved system operation.

Acknowledgments

The authors acknowledge financial support from the Guangdong Science and Technology Department (2021A0505030065).

Nomenclature

Sets and Indices

e	Equipment
$EACEVA$	Set of evaporators in AC system
$EACP$	Set of pumps in AC system
$ECCHP$	Set of subsystems in CCHP system
EWP	Set of water pumps
m	Reaction
PT	Set of products
$RMSR$	Set of reactions in MSR system
RT	Set of reactants
s	Stream
SFC	Set of streams in PEMFC
$SFCI$	Set of streams at the inlet of PEMFC
$SFCO$	Set of streams at the outlet of PEMFC
$SMSR$	Set of streams in MSR system
$SMSRI$	Set of streams at the inlet of MSR system
$SMSRO$	Set of streams at the outlet of MSR system
u	Substance

UFC	Set of substances in PEMFC
$UFCI$	Set of substances at the inlet of PEMFC
$UFCO$	Set of substances at the outlet of PEMFC
$UMSR$	Set of substances in MSR system
Parameters	
CRF	Capital recovery factor
C_s^T	Total surface concentration at active site (mol/m^2)
$ex_{\mathrm{CH_3OH}}$	Molar chemical exergy of methanol at standard condition (J/mol)
$HHV_{\mathrm{CH_3OH}}$	Higher heating value of methanol (J/mol)
$HHV_{\mathrm{H_2}}$	Higher heating value of hydrogen (J/mol)
$LH_{\mathrm{H_2O}}$	Latent heat of water (J/mol)
m^{cat}	mass of catalyst (kg)
n^{FC}	Number of single fuel cells in PEMFC stack
p^{ref}	Reference pressure (kPa)
R	Ideal gas constant (J/(mol·K))
S^c	Surface area per unit mass catalyst (m^2/kg)
T^{amb}	Ambient temperature (K)
$T^{hotw,out}$	Outlet temperature of hot water (K)
T^{ref}	Reference temperature (K)
t^{opr}	Annual operation time (h/yr)
$UC_{\mathrm{CH_3OH}}$	Unit cost of methanol ($/mol)
$UC_{\mathrm{H_2O}}$	Unit cost of water ($/mol)
$v_{m,u}$	Stoichiometric number of substance u in reaction m
ΔT^{MIN}	Minimum approach temperature (K)
$\Delta_f h_u^0$	Standard molar enthalpy of formation (J/mol)
$\Delta_f s_u^0$	Standard molar entropy of formation (J/(mol·K))
η^{pump}	Isentropic efficiency of pump
ρ^b	Density of catalyst (kg/m^3)
Continuous variables	
C^{fuel}	Fuel cost ($/yr)

678 C^{opr} Operating cost ($/yr)

679 $C^{tot,inv}$ Total investment ($)

680 C_e^{inv} Investment cost of equipment e ($)

681 $CP_{s,u}$ Heat capacity of substance u in stream s (J/(mol·K))

682 $E^{FC,Nerst}$ Nerst potential of single fuel cell (V)

683 Ex^{coldw} Exergy of cold water (W)

684 Ex^{hotw} Exergy of hot water (W)

685 $Ex_{\mathrm{CH_3OH}}$ Chemical exergy of methanol (W)

686 $f_{s,u}$ Molar flow rate of substance u in stream s (mol/s)

687 $f_{\mathrm{CH_3OH}}^{MSR,in}$ molar flow rate of methanol in feed to reactor (mol/s)

688 $g_{s,u}$ Molar Gibbs free energy of substance u in stream s (J/mol)

689 I^{FC} Current (A)

690 i^{FC} Current density (A/m^2)

691 K_m Chemical equilibrium constant

692 K_u^* Adsorption coefficient of intermediate u

693 k_m^{rate} Rate constant of reaction m

694 $LCOE$ Levelized cost of electricity ($/kWh)

695 m^{hotw} Mass flow rate of hot water (kg/s)

696 $mh_{s,u}$ Molar enthalpy of substance u in stream s (J/mol)

697 $ms_{s,u}$ Molar entropy of substance u in stream s (J/(mol·K))

698 p^{FC} Operating pressure of fuel cell (kPa)

699 p^{MSR} Reaction pressure in MSR system (kPa)

700 p_u Partial pressure of substance u (kPa)

701 p_u^e Effective partial pressure of substance u in PEMFC (kPa)

702 Q^{coldw} Cooling load of cold water (W)

703 Q^{hotw} Heating load of hot water (W)

704 $Q^{net,FC}$ Net heat output (W)

705 $Q^{sl,FC}$ Latent and sensible heat (W)

706 $Q^{tot,FC}$ Total energy output from PEMFC (W)

707 Q_e Heating load of equipment e (W)

708	r_m	Rate of reaction m (mol/(s·m^2))
709	T^{FC}	Operating temperature of PEMFC (K)
710	T^{MSR}	Reaction temperature in MSR system (K)
711	V^{FC}	Output voltage (V)
712	W^{CT}	Power consumption of cooling tower (W)
713	W^{FC}	Total electricity output of PEMFC (W)
714	W^{net}	Net power output (W)
715	W^{rfp}	Power consumption of reactant feed pump (W)
716	W_e	Power consumption of equipment e (W)
717	$xcom_u$	Molar fraction of substance u
718	Δf_u^{FC}	Molar flow rate change of substance u in PEMFC (mol/s)
719	Δf_u^{tot}	Total consumption of substance u in CCHP system (mol/s)
720	Δg_m^0	Molar Gibbs free energy change of reaction m (J/mol)
721	$\Delta V^{FC,act}$	Activation polarization loss (V)
722	$\Delta V^{FC,conc}$	Concentration polarization loss (V)
723	$\Delta V^{FC,ohm}$	Ohmic polarization loss (V)
724	η^{ele}	Net electrical efficiency
725	$\eta^{ex,sys}$	System exergy efficiency
726	η^{sys}	System energy efficiency
727	**Abbreviation**	
728	AC	Absorption cooling
729	CCHP	Combined cooling, heating and power
730	CHP	Combined cooling and heating
731	C-CCHP	Conventional combined cooling, heating and power
732	HEN	Heat exchanger network
733	MINLP	Mixed-integer nonlinear programming
734	MSR	Methanol steam reforming
735	PEMFC	Proton exchange membrane fuel cell
736	PI-CCHP	Combined cooling, heating and power with process integration
737	PSA	Pressure swing adsorption

Reference

Ahmadi, M.H., Mohammadi, A., Pourfayaz, F., Mehrpooya, M., Bidi, M., Valero, A., Uson, S., 2016. Thermodynamic analysis and optimization of a waste heat recovery system for proton exchange membrane fuel cell using transcritical carbon dioxide cycle and cold energy of liquefied natural gas. J Nat Gas Sci Eng 34, 428-438.

Al-Nimr, M.A., Bukhari, M., Mansour, M., 2017. A combined CPV/T and ORC solar power generation system integrated with geothermal cooling and electrolyser/fuel cell storage unit. Energy 133, 513-524.

Arsalis, A., 2019. A comprehensive review of fuel cell-based micro-combined-heat-and-power systems. Renew Sust Energ Rev 105, 391-414.

Asensio, F.J., Martín, J.I.S., Zamora, I., Garcia-Villalobos, J., 2017. Fuel cell-based CHP system modelling using Artificial Neural Networks aimed at developing techno-economic efficiency maximization control systems. Energy 123, 585-593.

Authayanun, S., Saebea, D., Patcharavorachot, Y., Arpornwichanop, A., 2014. Effect of different fuel options on performance of high-temperature PEMFC (proton exchange membrane fuel cell) systems. Energy 68, 989-997.

Baroutaji, A., Arjunan, A., Robinson, J., Wilberforce, T., Abdelkareem, M.A., Olabi, A.G., 2021. PEMFC Poly-Generation Systems: Developments, Merits, and Challenges. Sustain 13, 11696.

BP, Statistical review of world energy 2022. https://www.bp.com/en/global/corporate/energy-economics/statistical-review-of-world-energy.html

Buonomano, A., Calise, F., d'Accadia, M.D., Palombo, A., Vicidomini, M., 2015. Hybrid solid oxide fuel cells−gas turbine systems for combined heat and power: A review. Appl Energy 156, 32-85.

Chang, H., Wan, Z., Zheng, Y., Chen, X., Shu, S., Tu, Z., Chan, S., Chen, R., Wang, X., 2017a. Energy- and exergy-based working fluid selection and performance analysis of a high-temperature PEMFC-based micro combined cooling heating and power system. Appl Energy 204, 446-458.

Chang, H., Wan, Z., Zheng, Y., Chen, X., Shu, S., Tu, Z., Chan, S., 2017b. Energy analysis of a hybrid PEMFC−solar energy residential micro-CCHP system combined with an organic Rankine cycle and vapor compression cycle. Energ Convers Manage 142, 374-384.

Chen, J., Yan, L., Song, W., Xu, D., 2018a. Comparisons between methane and methanol steam reforming in thermally integrated microchannel reactors for hydrogen production: A computational fluid dynamics study. Int J Hydrog Energy 43, 14710-14728.

Chen, X., Gong, G., Wan, Z., Luo, L., Wan, J., 2015. Performance analysis of 5 kW PEMFC-based residential micro-CCHP with absorption chiller. Int J Hydrog Energy 40, 10647-10657.

775 Chen, X., Gong, G., Wan, Z., Zhang, C., Tu, Z., 2016. Performance study of a dual power source
776 residential CCHP system based on PEMFC and PTSC. Energ Convers Manage 119, 163-
777 176.
778 Chen, X., Zhou, H., Li, W., Yu, Z., Gong, G., Yan, Y., Luo, L., Wan, Z., Ding, Y., 2018b. Multi-
779 criteria assessment and optimization study on 5 kW PEMFC based residential CCHP system.
780 Energ Convers Manage 160, 384-395.
781 Chen, X., Zhou, H., Yu, Z., Li, W., Tang, J., Xu, C., Ding, Y., Wan, Z., 2020. Thermodynamic
782 and economic assessment of a PEMFC-based micro-CCHP system integrated with
783 geothermal-assisted methanol reforming. Int J Hydrog Energy 45, 958-971.
784 Ellamla, H.R., Staffell, I., Bujlo, P., Pollet, B.G., Pasupathi, S., 2015. Current status of fuel cell
785 based combined heat and power systems for residential sector. J Power Sources 293, 312-
786 328.
787 Ercolino, G., Ashraf, M.A., Specchia, V., Specchia, S., 2015. Performance evaluation and
788 comparison of fuel processors integrated with PEM fuel cell based on steam or autothermal
789 reforming and on CO preferential oxidation or selective methanation. Appl Energy 143,
790 138-153.
791 Fan, L., Tu, Z., Luo, X., Chan, S., 2022. MW cogenerated proton exchange membrane fuel cell
792 combined heat and power system design for eco-neighborhoods in North China. Int J
793 Hydrog Energy 47, 4033-4046.
794 Florides, G.A., Kalogirou, S.A., Tassou, S.A., Wrobel, L.C., 2003. Design and construction of a
795 LiBr-water absorption machine. Energ Convers Manage 44, 2483-2508.
796 Gao, P., Li, W., Cheng, Y., Tong, Y., Dai, Y., Wang, R., 2014. Thermodynamic performance
797 assessment of CCHP system driven by different composition gas. Appl Energy 136, 599-
798 610.
799 Ge, Y., Han, J., Zhu, X., Zhu, W., Yang, J., 2023. A combined cooling, heating and power
800 system with energy storage of waste heat to hydrogen. Appl Therm Eng 225, 120224.
801 Jannelli, E., Minutillo, M., Perna, A., 2013. Analyzing microcogeneration systems based on LT-
802 PEMFC and HT-PEMFC by energy balances. Appl Energy 108, 82-91.
803 Jin, Y., Sun, L., Shen, J., 2019. Thermal economic analysis of hybrid open-cathode hydrogen
804 fuel cell and heat pump cogeneration. Int J Hydrog Energy 44, 29692-29699.
805 Liang, Y., Chen, J., Yang, Z., Chen, J., Luo, X., Chen, Y., 2021a. Economic-environmental
806 evaluation and multi-objective optimization of supercritical CO2 based-central tower
807 concentrated solar power system with thermal storage. Energ Convers Manage 238, 114140.
808 Liang, Y., Hui, C.W., Luo, X., Chen, J., Yang, Z., Chen, Y., 2021b. A general mixed-integer
809 programming framework for efficient modeling, integration and optimization of
810 thermodynamic cycle-based energy systems. Energ Convers Manage 250, 114905.
811 Liang, Z., Liang, Y., Luo, X., Chen, J., Yang, Z., Wang, C., Chen, Y., 2022a. Synthesis and

simultaneous optimization of multi-heat source multi-pressure evaporation organic Rankine cycle with mixed working fluid. Energ Convers Manage 251, 114930.
Liang, Z., Liang, Y., Luo, X., Chen, J., Yang, Z., Wang, C., Chen, Y., 2022b. Superstructure-based mixed-integer nonlinear programming framework for hybrid heat sources driven organic Rankine cycle optimization. Appl Energy 307, 118277.
Liu, T., Liu, Q., Lei, J., Sui, J., Jin, H., 2018. Solar-clean fuel distributed energy system with solar thermochemistry and chemical recuperation. Appl Energy 225, 380-391.
Loreti, G., Facci, A.L., Baffo, I., Ubertini, S., 2019. Combined heat, cooling, and power systems based on half effect absorption chillers and polymer electrolyte membrane fuel cells. Appl Energy 235, 747-760.
Loreti, G., Facci, A.L., Ubertini, S., 2021. High-Efficiency Combined Heat and Power through a High-Temperature Polymer Electrolyte Membrane Fuel Cell and Gas Turbine Hybrid System. Sustain 13, 12515.
Mamaghani, A.H., Najafi, B., Casalegno, A., Rinaldi, F., 2016. Long-term economic analysis and optimization of an HT-PEM fuel cell based micro combined heat and power plant. Appl Therm Eng 99, 1201-1211.
Mamaghani, A.H., Najafi, B., Casalegno, A., Rinaldi, F., 2018. Optimization of an HT-PEM fuel cell based residential micro combined heat and power system: A multi-objective approach. J Clean Prod 180, 126-138.
Marandi, S., Sarabchi, N., Yari, M., 2021. Exergy and exergoeconomic comparison between multiple novel combined systems based on proton exchange membrane fuel cells integrated with organic Rankine cycles, and hydrogen boil-off gas subsystem. Energ Convers Manage 244, 114532.
Mert, S.O., Dincer, I., Ozcelik, Z., 2007. Exergoeconomic analysis of a vehicular PEM fuel cell system. J Power Sources 165, 244-252.
Peppley B.A., 1997. A comprehensive kinetic model of methanol-steam reforming on Cu/ZnO/Al2O3 catalyst. Doctor of philosophy. Royal Military College of Canada, Kinston, Ontario, Canada.
Peppley, B.A., Amphlett, J.C., Kearns, L.M., Mann, R.F., 1999. Methanol-steam reforming on Cu/ZnO/Al2O3 catalysts. Part 2. A comprehensive kinetic model. Appl Catal A-GEN 179, 31-49.
Prendl, L., Schenzel, K., Hofmann, R., 2021. Simultaneous integration of heat pumps and different thermal energy storages into a tightened multi-period MILP HENS superstructure formulation for industrial applications. Comput Chem Eng 147, 107237.
Radenahmad, N., Azad, A.T., Saghir, M., Taweekun, J., Bakar, M.S.A., Reza, M.S., Azad, A.K., 2020. A review on biomass derived syngas for SOFC based combined heat and power application. Renew Sust Energ Rev 119, 109560.

Safari, F., Dincer, I., 2020. A review and comparative evaluation of thermochemical water splitting cycles for hydrogen production. Energ Convers Manage 205, 112182.

Sarabchi, N., Mahmoudi, S.M.S., Yari, M., Farzi, A., 2019. Exergoeconomic analysis and optimization of a novel hybrid cogeneration system: High-temperature proton exchange membrane fuel cell/Kalina cycle, driven by solar energy. Energ Convers Manage 190, 14-33.

Su, B., Han, W., He, H., Jin, H., Chen, Z., Yang, S., 2020. A biogas-fired cogeneration system based on chemically recuperated gas turbine cycle. Energ Convers Manage 205, 112394.

Sun, L., Jin., Y., Shen, J., You, F., 2021. Sustainable Residential Micro-Cogeneration System Based on a Fuel Cell Using Dynamic Programming-Based Economic Day-Ahead Scheduling. ACS Sustainable Chem Eng 9, 3258-3266.

Sun, Y., Xu, C., Xu, G., Zhang, H., Li, B., Yang, Y., 2019. A comprehensive thermodynamic analysis of load‐flexible CHP plants using district heating network. Int J Energy Res 43, 4613-4629.

Wang, J., Han, Z., Guan, Z., 2020. Hybrid solar-assisted combined cooling, heating, and power systems: A review. Renew Sust Energ Rev 133, 110256.

Wang, J., Wu, J., Xu, Z., Li, M., 2017. Thermodynamic performance analysis of a fuel cell trigeneration system integrated with solar-assisted methanol reforming. Energ Convers Manage 150, 81-89.

Wu, C.W., Zhang, W., Han, X., Zhang, Y.X., Ma, G.J., 2020. A systematic review for structure optimization and clamping load design of large proton exchange membrane fuel cell stack. J Power Sources 476, 228724.

Wu, W., Zhai, C., Sui, Y., Zhang, H., 2021. A novel distributed energy system using high-temperature proton exchange membrane fuel cell integrated with hybrid-energy heat pump. Energ Convers Manage 235, 113990.

Xie, D., Wang, Z., Jin, L., Zhang, Y., 2012. Energy and exergy analysis of a fuel cell based micro combined heat and power cogeneration system. Energ Buildings 50, 266-272.

Xu, D., Liu, Q., Lei, J., Jin, H., 2015. Performance of a combined cooling heating and power system with mid-and-low temperature solar thermal energy and methanol decomposition integration. Energ Convers Manage 102, 17-25.

Zhao, J., Cai, S., Huang, X., Luo, X., 2021. 4E analysis and multiobjective optimization of a PEMFC-based CCHP system with dehumidification. Energ Convers Manage 248, 114789.

Zhao, J., Cai, S., Luo, X., Tu, Z., 2022a. Dynamic characteristics and economic analysis of PEMFC-based CCHP systems with different dehumidification solutions. Int J Hydrog Energy 47, 11644-11657.

Zhao, J., Cai, S., Luo, X., Tu, Z., 2022b. Multi-stack coupled energy management strategy of a PEMFC based-CCHP system applied to data centers. Int J Hydrog Energy 47, 16597-16609.

Zhao, J., Chang, H., Luo, X., Tu, Z., Chan, S.H., 2022c. Dynamic analysis of a CCHP system based on fuel cells integrated with methanol-reforming and dehumidification for data centers. Appl Energy 309, 118496.

Zhao, S., Ge, Z., Sun, J., Ding, Y., Yang, Y., 2019. Comparative study of flexibility enhancement technologies for the coal-fired combined heat and power plant. Energ Convers Manage 184, 15-23.